institut de physique nucléaire

LABORATOIRE ASSOCIÉ A L'IN2P3

UNIVERSITÉ PARIS-SUD
I.P.N. BP n° 1 - 91406 ORSAY

IPNO-DRE 84.02

SOLID STATE PHYSICS AND ACTINIDE SPECTROSCOPY WITH $ThBr_4$ AND $ThCl_4$.

Michel GENET

SOLID STATE PHYSICS AND ACTINIDE SPECTROSCOPY WITH $ThBr_4$ AND $ThCl_4$

M. GENET

Laboratoire de Radiochimie, Institut de Physique Nucléaire
Université de Paris-Sud, B.P. N° 1, 91406 ORSAY Cedex, France

To be published in the "Handbook on the Physics and Chemistry of Actinides" (A.J. Freeman, G. Lander and C. Keller Editeurs)

1. INTRODUCTION.

$ThBr_4$ was synthetized for the first time by Nilson (1882), then, at the end of the nineteenth century, French chemists, Troost and Ouvrard (1889) obtained it in an anhydrous form by reaction between bromine and a mixture of thorium and carbon. At that time, such properties as the colour, the stoichiometry and the melting point were roughly examined. The synthesis of $ThCl_4$ was firstly reported by Berzelius (1829). During the first half of the twentieth century, very few new studies on $ThBr_4$ and $ThCl_4$ were published. In the 60's, interest concerning these halides became important due mainly to special applications to fused salt reactor projects. Among several types of thorium compounds considered for fuel, the halides were of interest because of their physical properties. $ThCl_4$ appeared as a good material for these reactor projects, but the project was cancelled and these studies were suspended However, we retain as a legacy a large number of phase diagrams of thorium-uranium compounds. During the same period, many new complexes were prepared and intensively studied from a structural point of view. A book written by Brown (1968) gives a complete review of this subject.

We began our work on $ThBr_4$ and $ThCl_4$ in the 70's during a study of the hot atom chemistry of protactinium (Carlier and Genet, 1972).

To investigate the chemical fate of protactinium 233 coming from the β^- desintegration of ^{233}Th, we had to prepare the isotope which is readily obtained by a nuclear reactor irradiation upon the following process :

$$^{232}Th(n, \gamma)^{233}Th \xrightarrow{\beta^-} {}^{233}Pa \xrightarrow{\beta^-}$$

The thorium salt should be soluble in water to simplify the chemical analysis of the protactinium oxidation states (four and five). The target material should also be anhydrous, so we choose thorium halides to be irradiated. After few hours of irradiation in the nuclear reactor, $ThBr_4$ gave rise to a very bright emission of a blue-violet light which lasted several days. We obviously wanted to know where this light was coming from and that was the first step of the interest we brought to this crystal during more than ten years. This interest led us from a simple luminescence effect to one of the most sophisticated concepts in solid state physics : the incommensurate phase.

2. SYNTHESIS AND CRYSTAL GROWTH.

2.1. The purpose and the choices.

At the beginning of those studies, it was realized that an important effort would be necessary to obtain large, pure and good quality crystals. The main difficulties were related to the hygroscopic nature and the radioactivity of the product.

Several attempts were made to use commercially available compounds, but we never succeeded in obtaining anhydrous compounds. So we decided to prepare them by our own synthetic methods and to produce them on a kilogram scale, taking into account that experiments with only few grams of a very hygroscopic salt are always very difficult to perform.

Among the methods reviewed by Brown (1968), we chose for the synthesis that one involving direct combination of the elements (Hussonnois et al., 1981). For the crystal growth, the Bridgman method was retained (Hussonnois et al., 1981) since, first, thorium halides have a melt congruently, and, secondly, their vapor pressures at the melting point are relatively high (Rand, 1975) (this eliminated some techniques like the Czochralski method) and, at last, because the mixing of compounds with radioactive elements to obtain doped crystals is easier with Bridgman method.

The high melting points of $ThBr_4$ and $ThCl_4$ indicate the necessity of maintaining the melt in silica ampoules.

2.2. Synthesis of $ThBr_4$ and $ThCl_4$.

Most of the methods quoted in the literature do not give these compounds in a pure form and a final purification process is always carried out ; futhermore, the production is obtained in a finely divided powder form which is unsuitable for the crystal growth. From these two points of view, the direct combination of very pure thorium with the purest halogen is more satisfactory. Under these conditions, products are readily obtained in a pure and a polycrystalline form made of association of large grains (several cubic millimeters). The direct reaction takes place in an evacuated silica tube positioned vertically in order to promote easy removal of the material from the production site by gravity instead of using the usual gas flow technique.

2.3. Reactive products.

Thorium metal rods are of nuclear grade, each weighting about 600

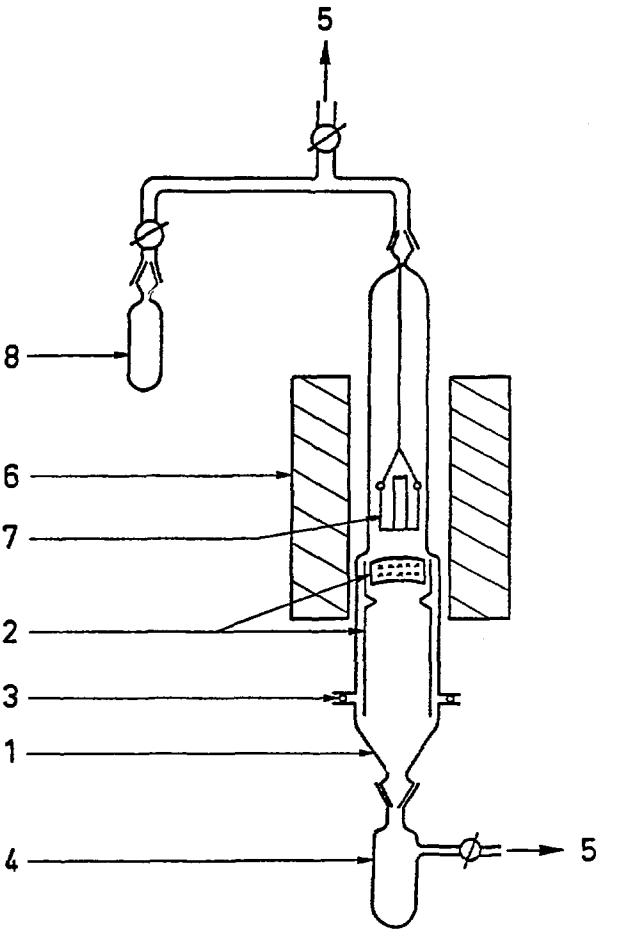

Fig. 1 - Schematic diagram of the synthesis reactor : 1 main silica tube ended by a pyrex cone, 2 lining silica tube and polycrystalline condensation position (×), 3 vitreous O ring, 4 recovery of the powder form, 5 to the vacuum line, 6 furnace, 7 vitreous carbon crucible and thorium or uranium rod, 8 bromide or chlorine tank.

grams. It is of interest to know that this thorium is 25 years old.

Bromine is a RP grade product (the reagent is degassed twice before use by freezing and pumping over the product at liquid nitrogen temperature).

Chlorine is delivered from a metallic gas container through a stainless steel manometer calibrated for absolute pressures. The purity is of 99.7 %.

2.4. Reactor device.

The reactor (fig. 1) is made of a silica tube (130 cm in length and 8.5 cm in inner diameter) which passes through an electrical furnace.

The upper part of the reactor can be linked via stop cocks either with a vacuum system or with a bromine or a chlorine tank. Thorium rods are placed in a vitreous carbon crucible and this is introduced through the lower part of the reactor. The crucible is then positioned to reside in the hottest zone of the furnace.

The main tube is lined by a second silica tube which facilitates the easy and fast recovery of the polycrystalline halide.

At the bottom, the reactor is connected to a funnel and to a pyrex ampoule to collect the powder form which falls down.

2.5. Procedure.

With the reactor closed, we pump at $\sim 10^{-4}$ torr for about 12 hours and in the meanwhile the furnace is heating until the reaction temperature is obtained. Then, the reactor is disconnected from the pumping system and we proceed to introduce the halogen gas (vapor pressure 200 torr for bromide and chlorine). The reaction :

$$Th + 2\ X_2 \longrightarrow ThX_4 \qquad X = Br \text{ or } Cl$$

starts immediately, giving the halide in a powder form during the first ten hours. Simultaneously, the polycrystalline form begins to be formed inside the lining tube below the crucible, as the powder production becomes over. Two days after thorium has entirely reacted, the heating is stopped and the reactor opened.

We obtain approximately one quarter powder and three quarters of polycrystalline material made of crystal of several cubic millimeters in size. The latter is quickly transferred to a dry glove box.

Table 1 - Values in part per million (ppm) of impurities in $ThBr_4$ obtained by a spark mass spectrometry analysis.

Al	12	Na	0.3
B	0.6	Nd	0.4
Ca	5	Ni	1.5
Ce	0.5	P	0.1
Cl	3	Pb	0.5
Co	0.05	Pr	0.05
Cr	1	Pt	2
Cu	3	S	3
F	4	Si	(500)
Fe	13	Ti	0.15
K	0.7	V	0.15
La	0.1	Zn	2
Mn	2		

Table 2 - Main synthesis features and crude physical properties of $ThBr_4$ and $ThCl_4$.

	$ThBr_4$	$ThCl_4$
Temperature reaction (°C)	850	900
Timing (days)	3	3
Colour	white	white
Yield (%)	90	90
UV Fluorescence	Blue	Blue pale
Melting point	679	760

2.6. Growth of pure crystals.

Only the polycrystalline product is used for the crystal growing. The growing tubes are silica ampoules. An ampoule is usually of few centimeters in diameter (up to 4 cm) and 10 centimeters in length. As these halides have a rather important supercooling effect, a small tip is blown onto the ampoule. This helps the crystal growth and prevents the product from being supercooled by the presence of the solidified material left in the tip. $ThBr_4$ and $ThCl_4$ are first melted under argon or helium atmosphere. After melting, the ampoule is evacuated and sealed.

To obtain crystal growth, the ampoule is lowered (0.5 cm per day) through an electrical furnace with a temperature gradient of 100° C per centimeter. We have also used a more sophisticated device with a rotation motion of 30 revolutions per minute and the same lowering speed. In this case, the furnace is a heat-pipe furnace loaded with metallic sodium. This apparatus allows us to get large and good quality crystals.

During cooling thermal strains in the crystal result in some cracked parts. The largest volumes obtained have been of several cubic centimeters.

Analysis of $ThBr_4$ single crystals by spark source mass spectrometry has been made. Values of impurities in ppm are given in table 1. They are related to the ThO_2 weight obtained from $ThBr_4$ crystals. The most important impurity element is silicon. Elements which are not mentioned correspond to an amount less than 0.05 ppm . The analytical method is not valid for uranium detection, nevertheless we know from our experiments that uranium is present in pure $ThBr_4$ and $ThCl_4$ crystals due to the fact that thorium ore (monazite) contains uranium. For $ThCl_4$, the silica ampoule is slowly attacked by the melt and we can expect a larger amount of silicon in the single crystals. The crystalline quality related to the defects and rate of dislocations has never been checked, but experiments performed with γ-ray diffraction technique (Freund and Schneider, 1972) ($\lambda = 0.03$ Å) give a less than 10 minutes mosaïc spread.

Some of the main features of the synthesis and of the product are shown in the table 2.

2.7. Growth of doped crystals.

As starting material we use pure $ThBr_4$ and $ThCl_4$ either in polycrystalline form or in single crystal. When it is possible, we try to use as the dopant material a compound having the same chemical composition as the matrix. For instance, we dope $ThBr_4$ with UBr_4 and $ThCl_4$ with UCl_4. We have determined that

UO_2 can be used interchangeably with the halides for doping crystal. Lanthanides are usually utilized as oxides.

For the crystal growth, the procedure is almost the same, excepted that the dopant is added to the pure material prior to the crystallization step. We noticed that the maximum dopant concentration, especially for 5 f elements, if often very small (less than 0.1 %). Segregation occurs when the growth rate is rather slow (0.5 cm per day).

The 5 f dopants were uranium as UBr_4, UCl_4 and UO_2, protactinium as Pa_2O_5 (twenty years old), neptunium as NpO_2 and NpF_4 and plutonium as PuO_2. For the 4 f, we have grown doped crystals with praseodymium as $PrBr_3$ or Pr_6O_{11}, neodymium, europium, gadolinium, erbium, thulium and ytterbium as sesquioxide.

2.8. Uranium content determination by a radiochemical process.

We need to know the actual uranium concentration in the doped crystal in many cases, for example, for the oscillator strength calculation. So, a special process has been devised to determine the uranium content of a crystal.

The uranium doped crystal is dissolved in an aqueous medium (HCl 10 N) and thorium-uranium separation is made by an exchange resin technique (Dowex AGI × 8, 200-400 mesh). Then, uranium is eluted by HCl 0.1 N and electrodeposited. Finally, the uranium amount is calculated from the α radioactivity measurement. The method has been tested using ^{233}U as a tracer. The efficiency of the recovery is greater than 95 %. In this way, we are able to measure concentrations of uranium in crystals as low as 20 ppm.

3. SPECIFIC PHYSICAL PROPERTIES OF PURE $ThBr_4$ AND $ThCl_4$.

We will mention here some of the properties that have been determined during these studies of $ThBr_4$ and $ThCl_4$.

3.1. Main characteristics of the crude crystal.

$ThBr_4$ and $ThCl_4$ are very transparent crystals. They are easily cleaved following a perpendicular face to the optical axis. The optical axis is very easy to find with a polarizing microscope. Both crystals are uniaxial and birefringent according to their crystalline structure. They can be polished, always in dry glove box with very fine polishing paper or cloth without any liquids. The polished faces are kept in good condition by keeping the crystals under helium atmosphere or under vacuum. Handling of the crystals without deterioration is only possible in a very dry metallic glove box (5 to 10 ppm of water vapor). Plastic boxes are not sufficiently air-tight.

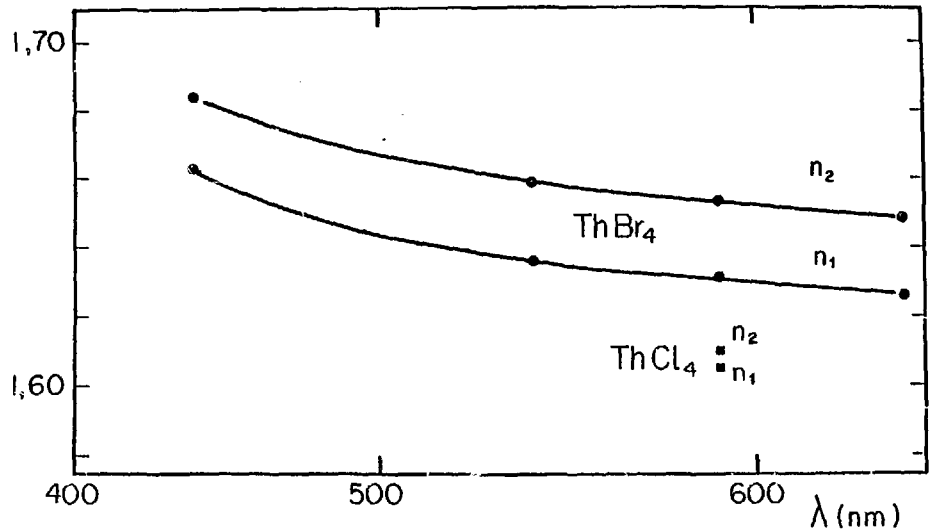

Fig. 2 - Refractive index variations with wavelength :
(o) $ThBr_4$, (■) $ThCl_4$.

Table 3 - Crystallographic data on $ThBr_4$ and $ThCl_4$.

	a(Å)	c(Å)	calculated density	Space group	Polymorphism	Reference
	8.473	7.468	4.63			Mooney (1949)
$ThCl_4$	8.490	7.483	4.60			Elson (1950)
	8.486	7.465	4.62			Mucker (1969)
(M = 373.85)	8.491	7.483	4.60	D_{4h}^{19}-$I4_1/amd$	β > 405° C	Brown (1973)
	6.408	12.924	4.68	$I4_1/a$	α < 405° C	Mason (1974)
	8.945	7.930	5.77			D'Eye (1950)
$ThBr_4$	8.939	7.964	5.76			Scaife (1966)
	8.931	7.963	5.77			Brown (1973)
(M = 551.65)	8.934	7.964	5.76	D_{4h}^{19}-$I4_1/amd$	β > 426° C	Mason (1973)
	6.737	13.601	5.94	$I4_1/a$	α < 426° C	Mason (1973)

3.2. Refractive indices.

The refractive indices have been measured in the visible range for $ThBr_4$ with an Abbe refractometer on a single crystal with two polished perpendicular faces, one being perpendicular to the optical axis. The incident wavelengths used are the classical emission lines of mercury (λ = 4350 Å and 5460 Å), thallium (λ = 5350 Å), sodium (λ = 5890 Å) and cadmium (λ = 6440 Å) lamps. The variation of both indices namely the ordinary n_1 and the extraordinary n_2 with wavelengths is shown on fig. 2. For $ThCl_4$, the measurement has been done only with the sodium lamp. For both crystals $n_2 > n_1$, so they are called optically positive.

3.3. Crystal structure of $ThBr_4$ and $ThCl_4$.

The crystallographic data available when we started this work have been summarized in the table 3.

We notice that $ThBr_4$ and $ThCl_4$ are tetragonal and isomorphous at room temperature (RT). They undergo a phase transition at higher temperature.

The single crystals prepared by the Bridgman method correspond to the high temperature β-phase for $ThBr_4$ and $ThCl_4$. A systematic research effort has been made to determine the structure of these crystals at low temperature. Using Raman spectroscopy and neutron scattering, we found out that $ThBr_4$ undergoes a phase transition at 95 K and $ThCl_4$ at 70 K. This was confirmed by other techniques like X-ray diffraction, EPR and NQR spectroscopy. This transition for $ThBr_4$ and $ThCl_4$ has been intensively studied because it determines the nature of the optical spectroscopy further made on 5 f elements.

3.4. Infrared and Raman studies.

The phase transition of $ThBr_4$ and $ThCl_4$, respectively at 95 and 70 K, were firstly seen by Raman spectroscopy. The complete determination of the phonon energies and their label symmetry have been explored (Hubert et al., 1981) to help the spectroscopical work on 5 f elements where numerous vibronic transitions had been observed. Infrared was performed on powder and single crystal by absorption and reflection. For Raman, we used single crystal in order to get a better assignment of the lines from polarized spectra.

As previously mentionned, $ThBr_4$ and $ThCl_4$ are isomorphous and belong to the D_{4h}^{19} space group with two molecules in the primitive unit cell. Optical activities expected to be seen by infrared and Raman spectroscopy (that

Table 4 - Label symmetry modes (at $q \neq 0$) for $ThBr_4$ and $ThCl_4$.

		Optic	Acoustic
Infrared active	A_{2u}	2	1
	E_u	3	1
Raman active	A_{1g}	2	-
	B_{1g}	3	-
	B_{2g}	1	-
	E_g	4	-
Inactive optically	A_{2g}	1	-
	A_{1u}	1	-
	B_{1u}	2	-
	B_{2u}	1	-

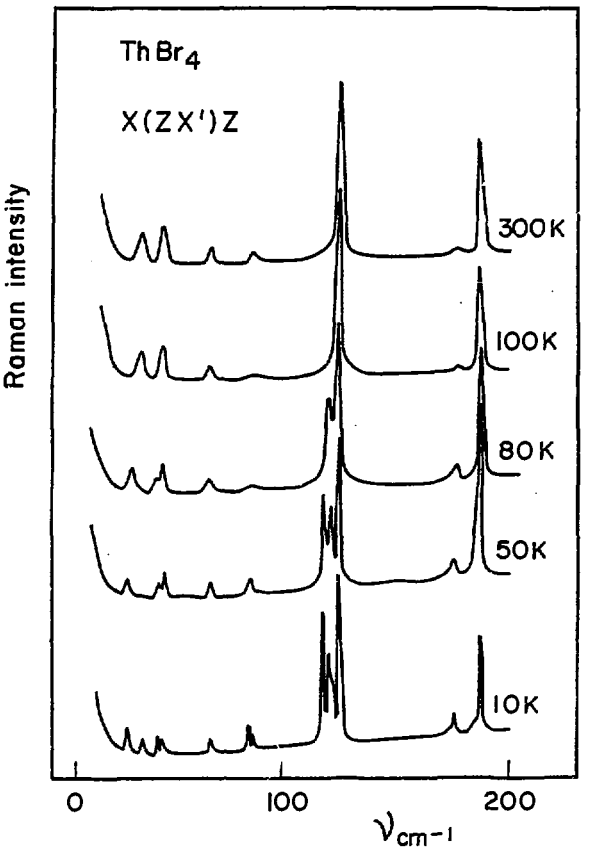

Fig. 3 - Raman spectra variations of $ThBr_4$ with temperature for the X(ZX')Z configuration.

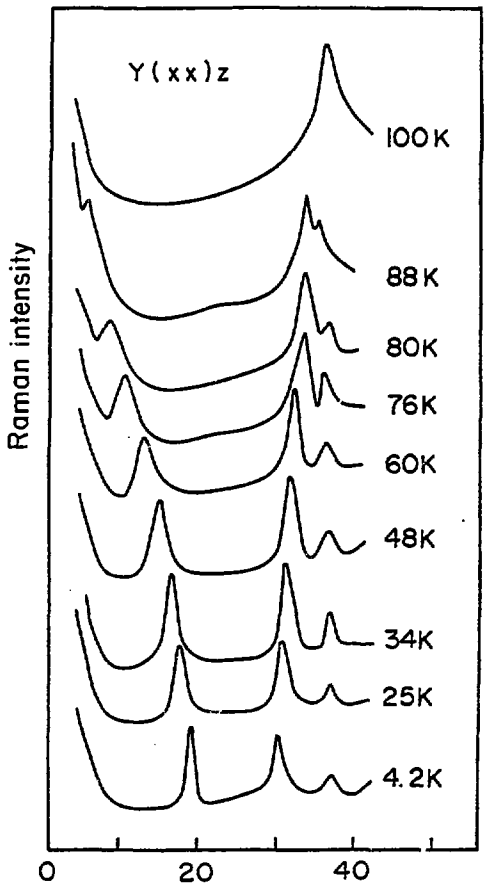

Fig. 4 - Temperature variation of the low frequency Raman spectra of $ThBr_4$ (Stokes' component).

Table 5 - Frequencies of the optically Raman and infrared active vibrations of $ThBr_4$ and $ThCl_4$ in cm^{-1} at RT and at 15 K.

	$ThBr_4$	$ThCl_4$	$ThBr_4$	$ThCl_4$
	at RT		at 15 K	
Soft mode	(0-20 cm^{-1})	(0-.....)		
E_g(R)	38	57	30	51
			38	
B_{1g}(R)	45	57	47	63
			48	67
			50	
B_{2g}(R)	66	70		
E_u(IR)	TO-66	TO-103	71	75
	LO-73	-		104
E_g(R)	82	98	90	107
E_u(IR)	TO-97	TO-134	93	
	LO-101			
A_{1g}(R)	108	181	118	182
				187
E_g(R)	122	188	125	193
			126	
			127	
A_{2u}(IR)	TO-125	TO-162	133	
B_{2g}(R)	135	214	-	214
A_{2u}(IR)	TO-155	-	-	
E_u(IR)	TO-160	TO-230		
	LO-180		184	
B_{2g}(R)	183	301		
E_g(R)	187	260		265
A_{1g}(R)	194	297	193	
			196	302

means at q = 0) for a D_{4h} factor group are given in table 4.

Upon the 30 total degeneracy of the vibration modes, 5 are infrared active, 10 are Raman active and 5 are inactive. Absorption spectra of powdered $ThBr_4$ and $ThCl_4$ at room temperature in the range 20-400 cm^{-1} show 5 bands. Difficulties, occuring in assignment of the observed bands, polarized IR reflectivity measurements, were attempted on a single crystal. The real and imaginary part of the complex dielectric constant were obtained using the Kramers-Kronig analysis and the transversal and longitudinal optical frequencies were calculated from the reflectance data for the E_u modes. Under these conditions, A_{2u} modes were deduced by difference from the powder absorption spectrum since it gives directly the TO frequencies values. Raman studies were done on $ThBr_4$ and $ThCl_4$ single crystals from room temperature to 15 K. These studies brought us important experimental results, namely the discovery of a phase transition at low temperature for $ThBr_4$ (T_c = 95 K) and for $ThCl_4$ (T_c = 70 K). In fact, below these temperatures, a new feature gradually appears. For example, fig. 3 shows the Raman spectrum behaviour from 300 K to 10 K for a given observation configuration (Delamoye et al., 1982a). Especially additional components are observed at frequencies close to that of the E_g modes at the high temperature phase. In the observation case, where the A_{1g} modes at the high temperature phase are observed (fig. 4), a particularly underdamped soft mode appears. The frequency of this soft mode versus temperature is monitored by the law $\omega = A(T_c - T)^{\beta}$, where T_c = 95 K is the transition temperature and β the critical exponent which is equal to 1/3.

Results of both infrared and Raman spectroscopy studies are reported in table 5.

3.5. X-ray diffraction at low temperature and neutron diffraction on powder.

For a better understanding of the phase transition, the X-ray diffraction was performed at 130, 77 and 10 K on the β-form finely ground (20 μ) in an helium cryostat (De Kouchkovsky et al., 1981). A special attention was brought to the dryness which was kept at 5 ppm of water during the sample preparation and the experiment. Thus the cryostat was loaded in the dry glove box. Patterns were obtained with the filtered K_α lines of the chromium and cobalt. In addition to the fundamental and allowed lines corresponding to the space group of β-$ThBr_4$, several very faint reflexions were observed at 10 K in agreement with a structural change. These two groups of lines can be indexed in the RT space group with a thermally shrinked cell (a = 6.916 Å ; c = 7.893 Å) for the strong lines, and the weak one could be considered coming from a supercell that is a

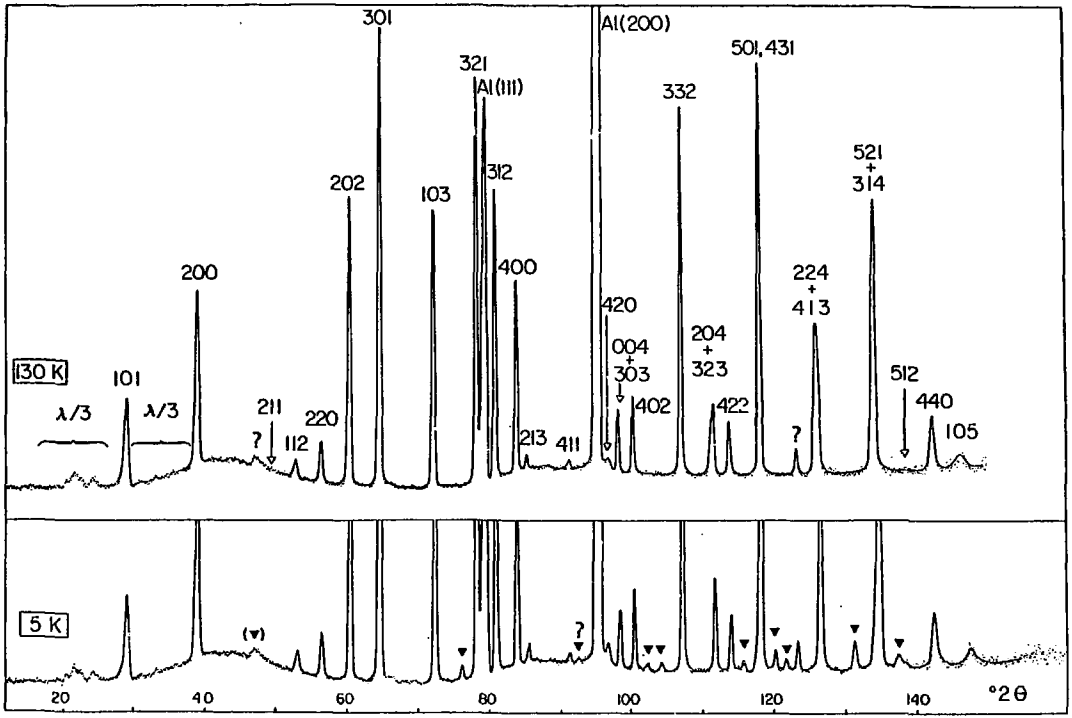

Fig. 5 - Neutron diffraction spectrum (λ = 2 986 Å) of β-$ThBr_4$ at 130 K and below the phase transition (at 5 K).

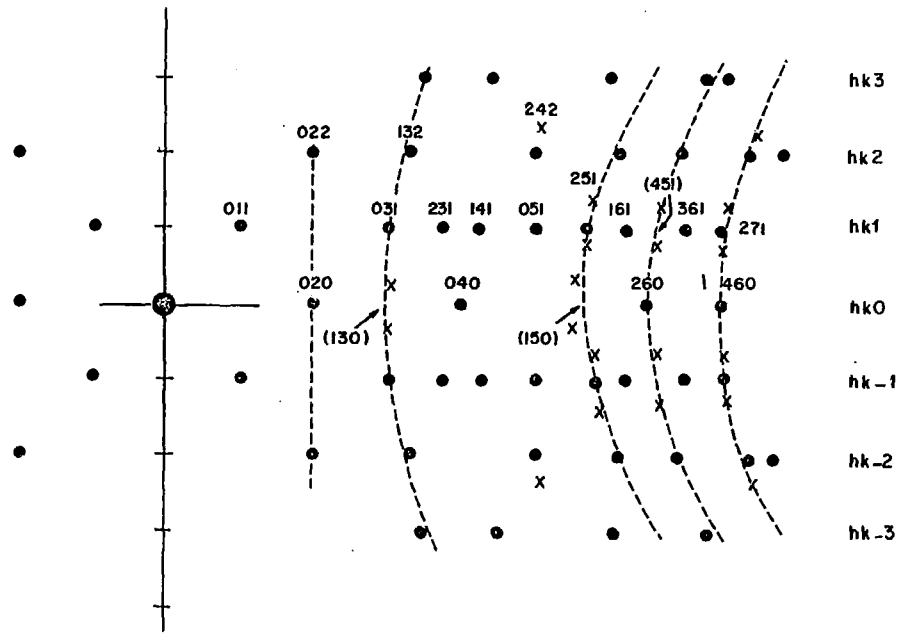

Fig. 6 - Satellite positions (×) appearing in $ThBr_4$ neutron diffraction pattern below the phase transition among the Bragg dots (●).

cell 2, 3, 4 ... times the initial one.

At first approximation, the additional powder lines could be indexed by tripling the unit cell along the tetragonal c axis. The weakness of the superstructure lines lead us to think that bromine displacements could be involved in the transition. Thus neutron diffraction were planned to increase the relative contribution of bromine atom. For X-ray, atomic coherent scattering length depends on the number of electrons and the intensity ratio for Th^{4+} and Br^- varies as $(\frac{f\ Th^{4+}}{f\ Br^-})^2$ which is 5 at $2\theta = 0°$ and increases to 8 at $2\theta = 150°$. For neutrons, this ratio is equal to 2 whatever the diffraction angle.

All neutron experiments were done at Grenoble at the Laue-Langevin Institute. Data obtained with the D1A diffractometer at 5 K and 130 K reproduced exactly the X-ray results with superstructure lines observed at the same position (fig. 5). They are a little more intense than on X-ray patterns, which confirms a larger bromine contribution. These results also showed that a very strong anisotropy appeared in the thermal shrinking, the relative variation of the lattice parameter c being 5 times larger than that of parameter a.

3.6. Neutron diffraction at low temperature on single crystals.

Single crystals experiments were performed with the D12 four circle diffractometer.

From a structural point of view, the four fold axis is maintained and oscillating patterns around the C_4 with the incident neutron beam perpendicular to it allow us to investigate diffraction by the planes h, k, l, with $l = 0, \pm 1, \pm 2...$ The place of the satellites in relation to the Bragg dots diffraction are shown on figure 6. We clearly see that satellite lines appear between planes corresponding to integer values for h, k, l. The intensities of the satellites are weak and their places are characterized by $l = n \pm \frac{1}{3}$.

It has been shown by Weissenberg patterns and further oscillating patterns around other axis that, for satellites, h and k always kept integer values while l had still non integer values. The resulting structural change being roughly described as a tripled unit cell along the c axis.

Accurate values of l were determined with the D10 four circle spectrometer giving :

$$l = n \pm \frac{1}{3}(1 - \delta)$$

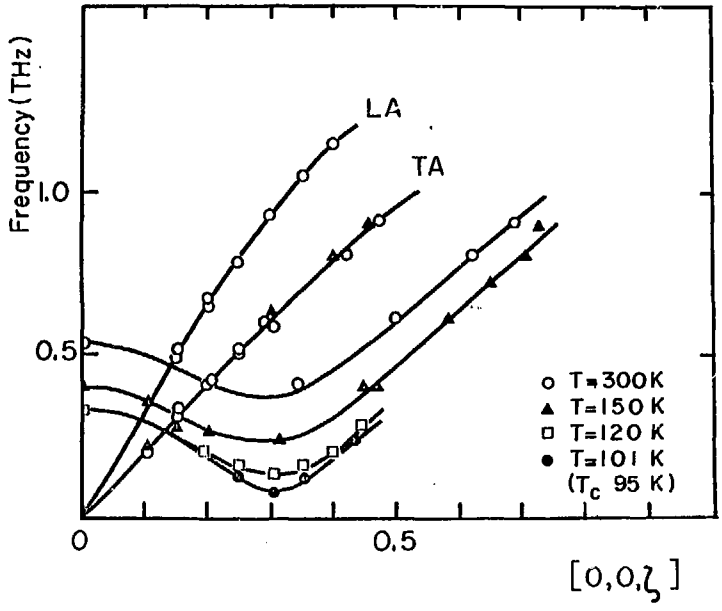

Fig. 7 - Dispersion curves for the LA, TA and soft optic modes versus temperature.

with $\delta = 0.063$, this value is almost constant from the phase transition temperature (T_c = 95 K for $ThBr_4$) down to 4 K.

So, the new phase didn't really appear as a real tripling of the tetragonal unit cell but as a series of cells along z direction, each of them different from the others in terms of atoms positions. Such a structure is called incommensurate. In $ThBr_4$, this incommensurate structure could be represented by a modulation whose wavevector q_s is directed along c axis with :

$$q_s = \frac{2\pi}{\lambda} = \frac{2\pi}{c} \cdot \frac{1}{3} (1 - \delta) = 0.310\ c^* \pm 0.005$$

As δ is inchanged from T_c = 95 K to 4 K, we can say that the new phase is still incommensurate in this wide range of temperatures without any lock-in (meaning that $\frac{q_s}{c^*}$ ratio remains irrational). This situation is not very common, and the crystal usually encounters a classical commensurate phase when the temperature is decreased. This particularity of $ThBr_4$ is quite interesting as the study of the incommensurate structure becomes possible over 90 K.

3.7. Inelastic neutron scattering and dynamics of the phase transition.

We already knew by Raman spectroscopy (Hubert et al., 1981), as previously reported, that $ThBr_4$ undergoes the transition with appearance at the low temperature phase of a soft mode whose energy decreases as the temperature of the crystal increases and becomes zero at the transition temperature (see 3.4.). Taking into account this previous observation, inelastic scattering experiments were planned to get more information on this particular vibration in the high $ThBr_4$ phase for which Raman spectroscopy is unable to give any data.

The crystal orientation was chosen to be (2, 3, 1) which corresponds to the (0, 0, 0) reduced Brillouin zone (in the following ξ being the reduced coordinate along c^*). Under these conditions we can observe simultaneously the soft optic mode and the transverse acoustic branch. The dispersion curve versus temperature (Bernard et al., 1983) is shown on fig. 7. We notice that the transverse acoustic branch slope and the longitudinal one measured in a separate experiment are almost unaffected for the $[0, 0, \xi]$ direction of the propagation. By cooling the crystal from RT to 95 K, we saw the energy of the soft mode, which passes through a minimum value. This value varies with temperature. It is $\xi = 0.28$ for T = 150 K and about $\xi = 0.30$ for the temperature transition T_c = 95 K. This corresponds to the freezing of the soft mode leading to the incommensurate phase.

For the low temperature domain, dynamics of the new phase in directly connected with the intensities of the satellite lines. Thus, the comparison of

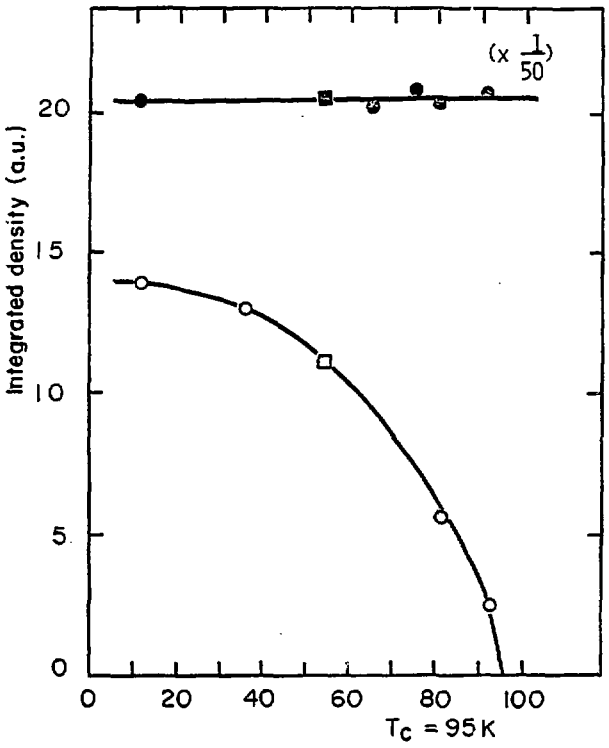

Fig. 8 - Temperature dependence of the (2, 3, 0, 69) satellite intensity (o) in comparison with that of the (2, 3, 1) fundamental line (•) (normalization between curves were made at 55 K).

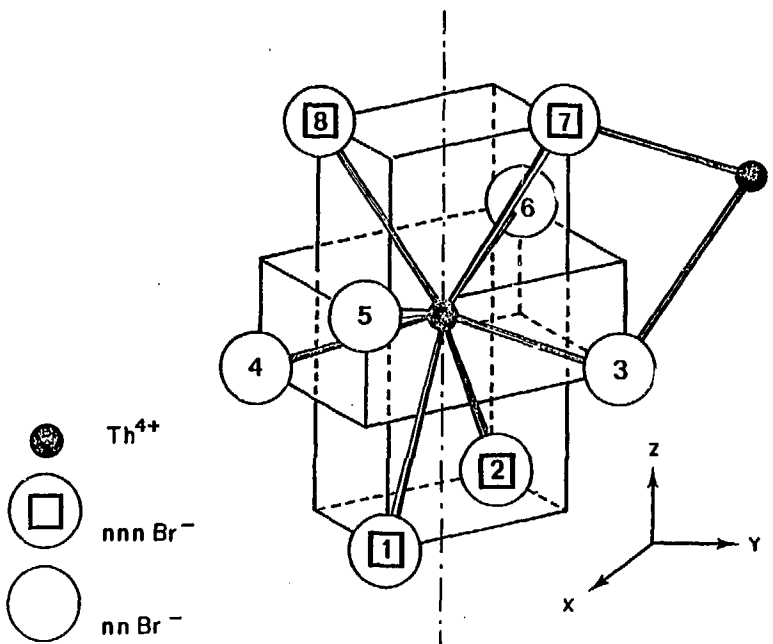

Fig. 9 - Perspective view of the β-$ThBr_4$ primitive unit cell (nn : nearest neighbour ; nnn : next nearest neighbour).

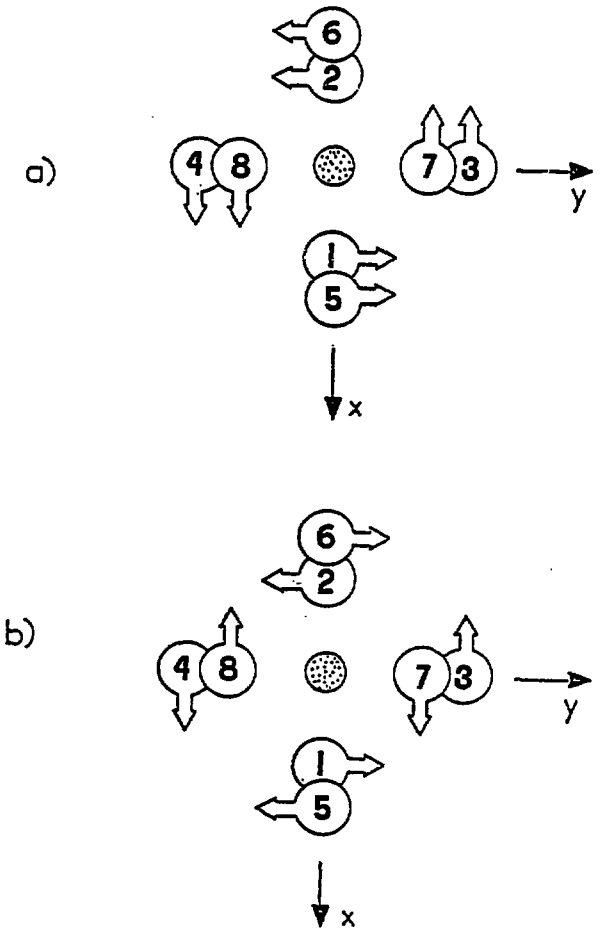

Fig. 10- Eigenvectors of B_{1u} (a) and B_{2g} (b) modes.

Table 6 - Cartesian components of Br^- positions vectors r_k^o and rotational eigenvectors e_k.

k	r_k^0	e_k
1	$\frac{1}{2} - x, 0, z - \frac{1}{4}$	0, 1, 0
2	$x - \frac{1}{2}, 0, z - \frac{1}{4}$	0, $\bar{1}$, 0
3	0, x, z	$\bar{1}$, 0, 0
4	0, $\bar{x}$, z	1, 0, 0
5	x, 0, $\bar{z}$	0, 1, 0
6	$\bar{x}$, 0, $\bar{z}$	0, $\bar{1}$, 0
7	$0, \frac{1}{2} - x, \frac{1}{4} - z$	$\bar{1}$, 0, 0
8	$0, x - \frac{1}{2}, \frac{1}{4} - z$	1, 0, 0

satellite intensity (2, 3, 0.69) with the intensity of the fundamental line (2, 3, 1) shown on fig. 8, indicates for T < 60 K a saturation effect which means that modulation amplitude remains small even at low temperature. It has been estimated that amplitude is of the order of few per cent of the cell edge (Bernard et al., 1983). Taking into account several experimental results like satellite extinction observation, or no interaction between the acoustic and optic modes, and also the normal mode decomposition obtained by Raman spectroscopy (Hubert et al., 1981), it has been possible to find out the symmetry label of the soft mode which is τ_4 in Kovalev (1964) notations. This irreducible representation belongs to the symmetry group of the wavevector q_s : C_{4v} built with the eight symmetry operations of the high temperature group which leaves q_s invariant. It is of interest to know the actual displacements of the atoms in the incommensurate phase, keeping in mind that thorium ions are not affected by a modulation of τ_4 symmetry, bromide ion positions are only to be considered. The τ_4 mode is a linear combination of B_{1u} (silent mode) and B_{2g} (Raman active mode) indexed at $q_s = 0$ with D_{4h} as the symmetry group of the wavevector for the high temperature phase. Referring to fig. 9 for atom indices, the two sets of eigenvectors (B_{1u} and B_{2g}), which are basis of τ_4 are shown on figure 10. One of them, B_{1u} corresponds to a rotational displacement around the C_4 axis, the other one, B_{2g}, being regarded as a twist deformation.

Under these conditions, assuming that the modulation is purely sinusoïdal, the single-plane-wave approximation states that the static ionic displacement $u_{\ell k}$ for the kth atom in the ℓth primitive cell is represented by :

$$u_{\ell k} = \eta \, e_k \cos (q_s \, r^o_{\ell k} - \varepsilon_k \, \theta) \qquad (1)$$

where η is an amplitude factor varying with temperature,

e_k is the unit vector along x or y,

$r^o_{\ell k} = r^o_\ell + r^o_k$ is the position vector of the kth atom in the lth primitive unit cell,

ε_k = + 1 for k = 1 to 4, and -1 for k = 5 to 8,

θ is an angle phase which controls the phase difference between bromide ions.

According to their labelled positions (k = 1 to 8) the e_k and r^o_k values for tetrabromide ions are given in table 6. The eight Br^- ions are chosen to be the nearest neighbours of a thorium atom located at the origin as shown in figure 9. From symmetry considerations it comes that the D_{2d} symmetry site of thorium ions

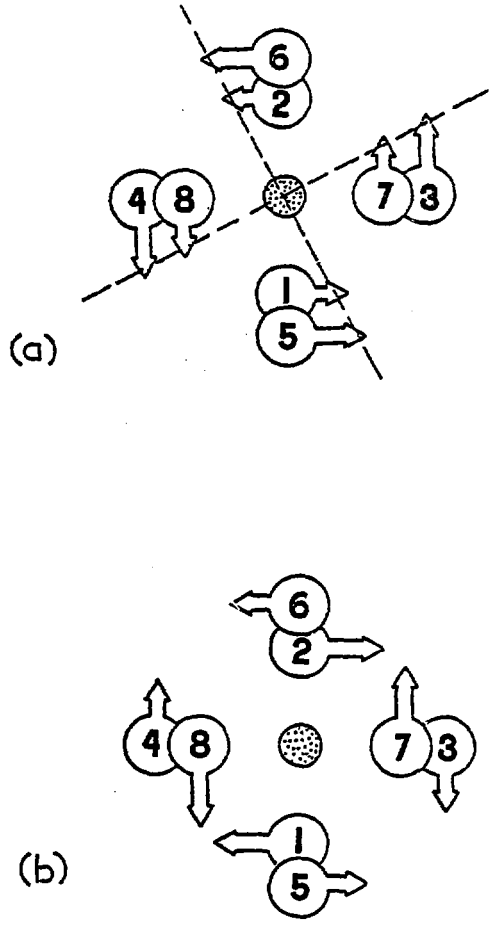

Fig. 11- Schematic representation of Br^- displacements for (a) : $\varphi_\ell \neq 0$ (symmetry D_{2d}) and for (b) : $\varphi_\ell \neq \frac{\pi}{2}$ (symmetry D_2).

Table 7 - Main features characterizing the phase transition of $ThBr_4$.

	β-$ThBr_4$	$\xrightarrow{T_c = 95\ K}$	$ThBr_4$ incommensurate
Space group	D_{4h}^{19}		
Vibration mode	B_{1u} silent B_{2g} (Raman active) $\Big\}\ \tau_4$		Freezing soft mode $\tau_4 \rightarrow aB_{1u} + bB_{2g}$ The condense wave is characterized by $u_{\ell k}$ stands for Br^- displacements η : amplitude of $u_{\ell k}$ few percent of the edge cell θ : phase angle 21° 6 (makes difference between $u_{\ell k}$ of a same cell). φ_ℓ : local phase. $0 < \lvert\varphi_\ell\rvert < \frac{\pi}{2}$ (makes difference between $u_{\ell k}$ of various cells.
Site symmetry for Th^{4+} ion	D_{2d}		$\varphi_\ell = 0$ D_{2d} $\varphi_\ell = \pm \frac{\pi}{2}$ D_2 $\varphi_\ell \neq 0 \neq \pm \frac{\pi}{2}$ D_2

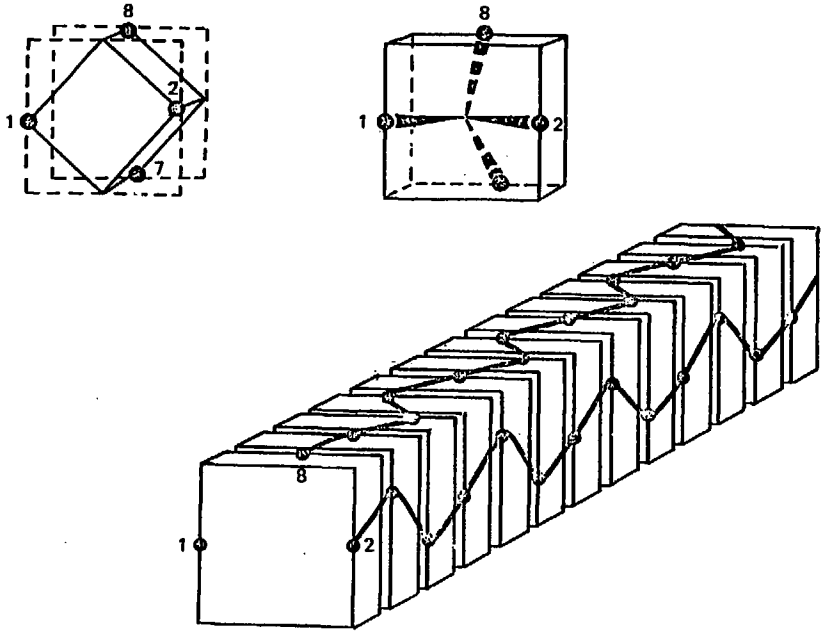

Fig. 12 - Schematic representation of the modulated bromine atom displacements (for k = 2 and 8). Thorium atoms are not shown.

in the RT phase could be broken into either D_2 or C_2 in the modulated phase. The local symmetry is inscribed through the phase angle value θ. From experimental data, this value is $20.2 \pm 3°$ (Delamoye at al., 1982b) and was calculated to be $21.6°$ for the D_2 symmetry. So we get a rather good agreement between what is theoretically drawn from the model used for displaced atoms and the experimental results. We shall assume that as this condition is sufficiently fulfilled at 4 K, the uranium site symmetry is effectively D_2.

With the help of table 6, and introducing the local phase angle $= \varphi_\ell$:

$$\varphi_\ell = q_s \cdot r_\ell^o \text{ (modulo } \pi)$$

we obtain :

$$(2) \qquad q_s\, r_{\ell k}^o = \varphi_\ell + q_s\, r_k^o = \varphi_\ell + \begin{cases} \pm 2\pi\xi z & \text{(for k = 3, 4, 5, 6)} \\ \pm 2\pi\xi \left(\frac{1}{4} - z\right) & \text{(for k = 1, 2, 7, 8)} \end{cases}$$

inserting (2) into (1) we obtain :

. for sites such as $\varphi_\ell \simeq 0$, the Br^- displacements correspond to a pure rotation by the same angle of the two bromide tetrahedra : the D_{2d} symmetry is maintained (fig. 11a).

. for sites such as $\varphi_\ell \simeq \pm \frac{\pi}{2}$, we obtain a pure twist deformation and the resulting site is D_2 (fig. 11b).

. for intermediate values of φ_ℓ both components are present and the corresponding site symmetry is still D_2.

The main features of the model which characterized the incommensurate structure of $ThBr_4$ is given in table 7.

To illustrate in a simple way how the modulation takes place in a series of unit cells, we have drawn on fig. 12 very schematically the combination of the B_{1u} and the B_{2g} modes. The unit cell is restricted to one set of bromide ions belonging to the same tetrahedra and we have just represented the cell as a box, the C_4 axis passing through Th^{4+} positions.

3.8. Existence of the τ_4 soft mode below T_c.

The existence of the soft mode in the low temperature phase is revealed by two kinds of results : Raman spectroscopy (Hubert et al., 1981) and inelastic neutron scattering (Bernard et al., 1983) which was unique in the incommensurate phase.

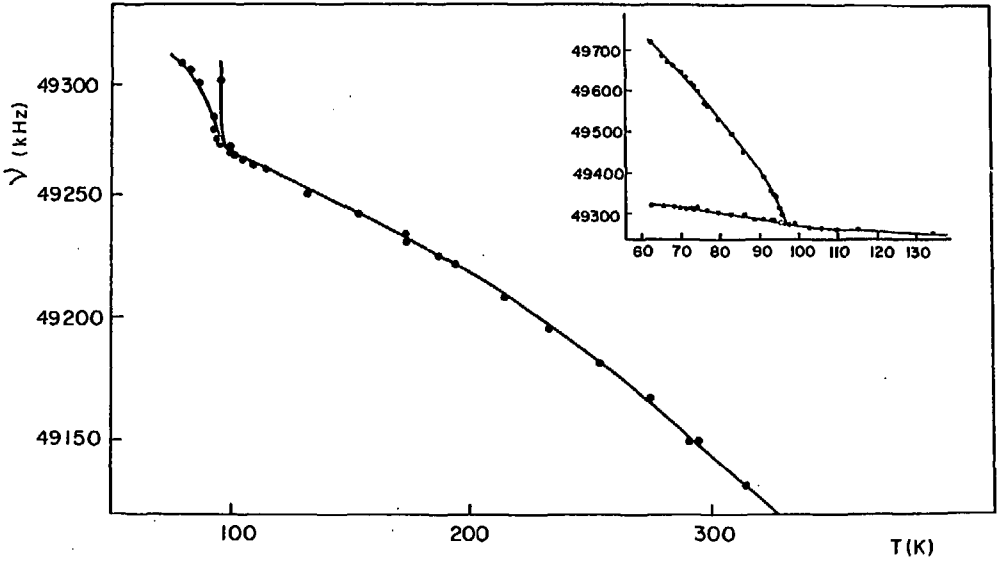

Fig. 13 - Temperature dependence of the ^{79}Br isotope NQR signal in $ThBr_4$.

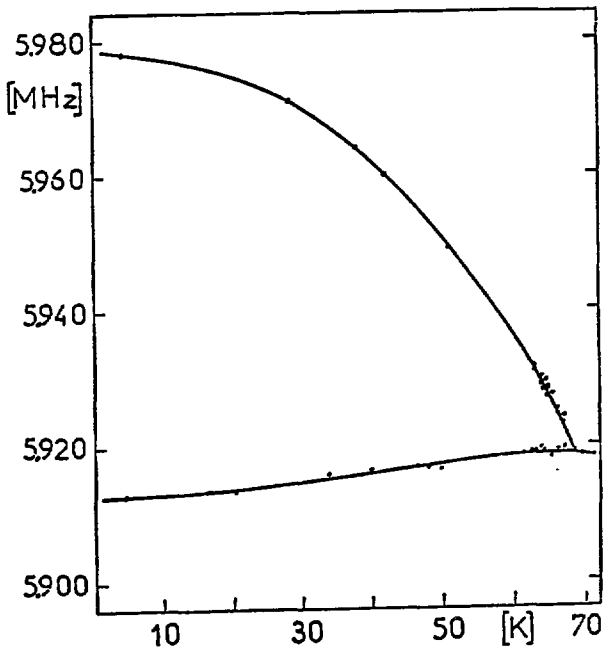

Fig. 14 - Temperature dependence of the ^{35}Cl isotope NQR signal in $ThCl_4$.

Below T_c, the τ_4 soft mode leads to two components in the incommensurate phase : the phase-mode in lower energy range and the amplitude-mode at higher energy (which is Raman active). Both of these branches have been studied for a given temperature (T = 81 K) in two different directions : $[0, 0, \xi]$ and $[2\xi, 3\xi, 0]$ from the origin of the Brillouin zone taken at (2, 3, 0.69). The extrapolated minimum value of the amplitude-mode at $\xi = 0$ has an energy of 0.24 THz, in good agreement with estimated values from the Raman data.

These very new results are related to the front line solid state physics field, $ThBr_4$ being the first example where amplitude-mode and phase-mode have been observed at the same time. The domain encountered is irrelevant to our subject. More details upon $ThBr_4$ will be found in the Bernard's (1983) paper, as for incommensurate phase, general and good introduction have been done by several authors (Currat, 1981), (Blinc et al., 1982), (Pynn, 1979). $ThCl_4$ crystals have never been examined by neutron diffraction yet, nevertheless, a lot of other experimental results let us think that this crystal would undergo, down 70 K, a transition of the same nature as $ThBr_4$ would.

3.9. Nuclear quadrupole resonance studies.

Investigation of $ThBr_4$ and $ThCl_4$ by Nuclear Quadrupole Resonance (NQR) technique was very tempting because both crystals are able to give a NQR signal through the impaired nucleon number for bromine (isotope 79 and 81) and for chlorine (isotope 35 and 37), all with a nuclear spin of I = 3/2. A study on $ThCl_4$ (Reddoch, 1961) was reported and it gives one site for chloride ion at room temperature and at 77 K. It is in agreement with the symmetry site of the halogen (C_s) at these temperatures. On the contrary, two independent studies on $ThBr_4$ (Carter, 1975), (Kravenchko et al., 1975) lead to many more sites than expected (4 to 5) at 300 K and 77 K, and do not mention any phase transition on $ThBr_4$. As a matter of fact, by working on Carter's own product, we could see one line split, indicating the presence of the phase transition. The extra lines observed at 300 K and 77 K haven't been interpreted yet.

As the Raman spectroscopy proved the existence of the phase transition, it was also interesting to study it by NQR spectroscopy. This has been done and it is effectively seen in figure 13 and 14, where the NQR frequency : ν_Q versus temperature is drawn for ^{79}Br and ^{35}Cl. The behaviour of both halides is very close with an increasing of ν_Q as temperature decreases until we reach the temperature phase transition T_c where two branches appear. For this temperature range,

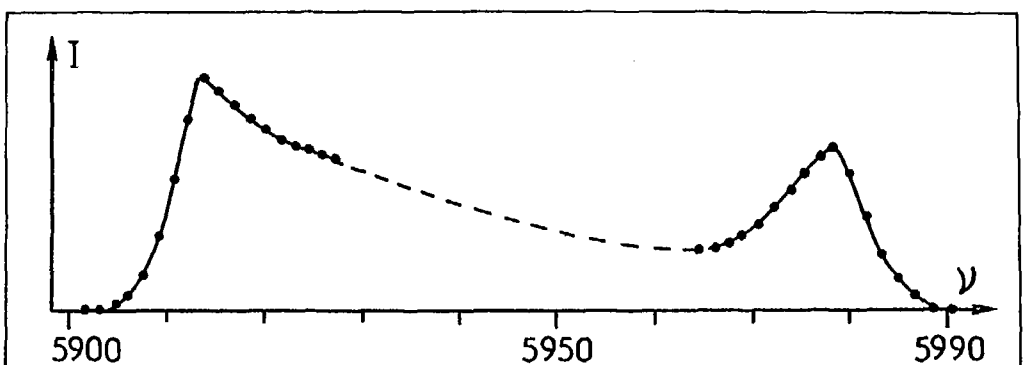

Fig. 15 - Asymmetrical shape of the ^{35}Cl NQR signals down the phase transition (intensity in arbitrary units).

Table 8 - Main luminescent characteristics of $ThBr_4$ and $ThCl_4$.

	$ThBr_4$	$ThCl_4$
Excitation threshold	3000 Å	2400 Å
Maximum wavelength excitation	2700 Å	2050 Å
Wavelength emission (broad band)	4050 Å	3450 Å
Lifetime	∿ 3 μs	∿ 5 μs
Quantum yield	∿ 0.9	∿ 0.9
Thermal quenching	350 K	425 K
Reference	(Carlier and Genet, 1975)	(Mentz, 1979)

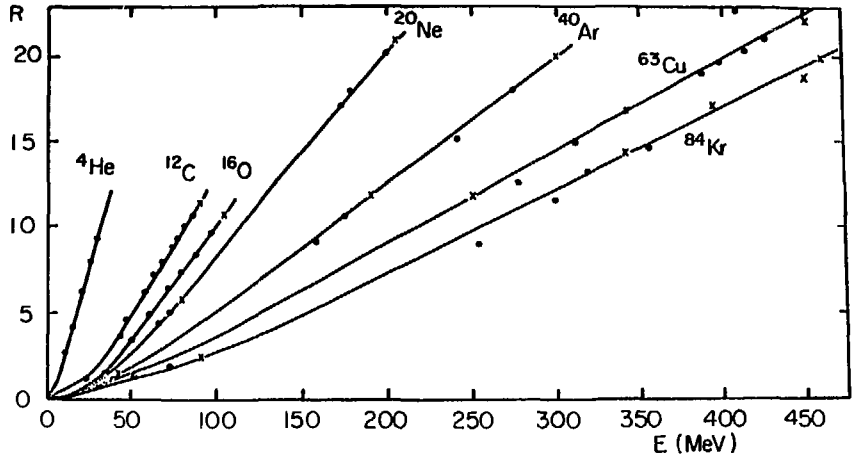

Fig. 16 - Response of $ThBr_4$ to heavy ions in function of energy.

the unique signal expected is observed. At lower temperature than T_c, we could imagine that we would get two kinds of symmetrysite . In fact, knowing the neutron diffraction results, the interpretation of the crow's foot-shaped double branch must obviously be started in connection with the dynamics of the incommensurate phase. Thus, it is actually thought that branches would be similar to the "edge-singularities" occuring in optical process (see 4.2.3.). The two extreme limits are separated by a continuum of ν_Q values as shown in figure 15 for ^{35}Cl.

Futhermore, the transition is found to be second order-like with a temperature dependence giving a critical exponent whose value of 1/3 is in good agreement with the incommensurate phase observed (Khan Malek et al. 1982).

3.10. Luminescent properties.

$ThBr_4$ and $ThCl_4$ are both fluorescent and radioluminescent compounds (Genet et al., 1976a). The fluorescence is obtained through the UV irradiation and the main features of this behaviour are summarized in table 8.

$ThBr_4$ is also phosphorescent, thermoluminescent and electroluminescent. These properties have been observed but not yet investigated.

The radioluminescence of $ThBr_4$ and $ThCl_4$ is observed at 4050 Å and 3750 Å respectively when they are excited by ionizing radiations (X and γ-rays) (Krupa et al., 1978), particles (e^-, α) (Hussonnois et al., 1977) or heavy ions (C^{4+} to Kr^{24+}) (Genet et al., 1975), (Genet et al., 1976b). Most experiments have been done with $ThBr_4$, but $ThCl_4$ would have shown the same behaviour.

The response of $ThBr_4$ to energetic heavy ions is given in figure 16. The main characteristics and comparison with NaI(Tl) to all kinds of particles and radiations usually encountered in nuclear physics, have been reported (Krupa and al., 1978). $ThBr_4$ appears as the heaviest and one of the most resistant scintillator known so far whose self-induced spectrum (see below) and high sensitivity towards water limit its practical uses. Nevertheless, its performances in nuclear particle detection and its capability of conversion of kinetic energy into light have been patented (French patent N° 75.19.961)(Genet et al., 1977a).

$ThBr_4$ has also been tested for fast neutron detection. These particles provoke the fission of thorium and the total kinetic energy of the fission products is registered through the scintillation of the crystal (Krupa et al., 1976). $ThBr_4$ acting as a scintillator and thorium being radioactive, this crystal emits

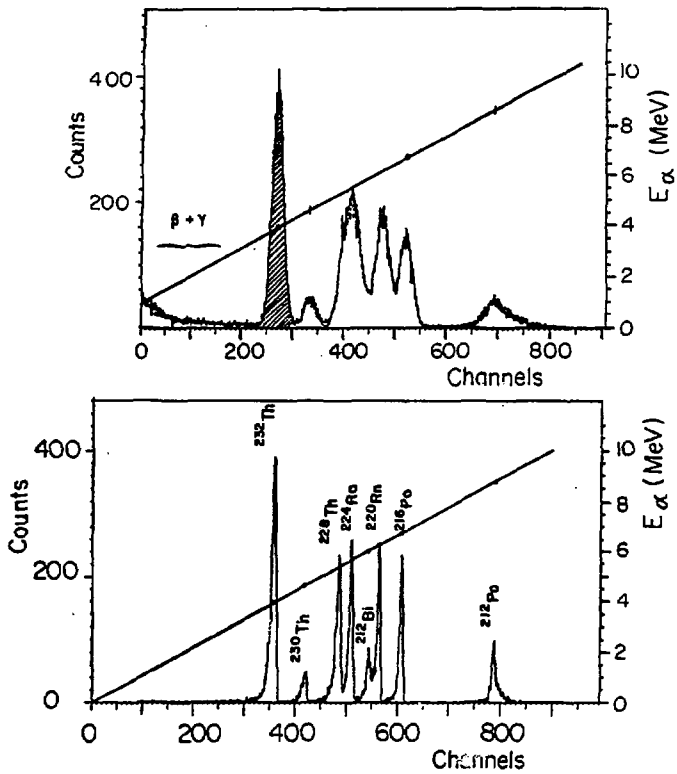

Fig. 17 - Self-induced α spectrum of $ThBr_4$ single crystal (upper curve) and α energy spectrum of electroplated thorium source measured with a Si-Au detector (lower curve).

light at 4050 Å without any excitation except its own. The careful analysis of the emission shows that it can be connected with the α-emitters of the 4 n thorium family. The peak identification was made through the comparison of self-induced α-spectrum of $ThBr_4$ with the α-spectrum of an electroplated thorium source measured with a Si-Au detector, as shown in figure 17 (Carlier et al., 1977). Taking into account the conversion yield for α-particles at a given energy, we can estimate that a $ThBr_4$ crystal of one cubic centimeter, according to the radioactive half-life of thorium (1.4×10^{10} years), is almost a permanent source of light which emits about 10^9 photons at 4050 Å per second over 4 π.

The luminescent properties of $ThBr_4$ and $ThCl_4$ were intensively studied, but the origin of this phenomenon is still unknown. We suppose that the mechanism could be related to a charge transfer between the electron of the bromide ion towards the thorium tetravalent ion. In terms of band structure, we could also say that the energy threshold of the fluorescence corresponds to the energy gap of the compound (∿ 4.6 eV), the electron-hole recombination leading to the luminescent effect. Any way, it seems that this effect is only due to a property of the crystal regardless of its state (powder, single crystal, vapor deposition film, etc). Under these conditions, we can say that it is an intrinsic fluorescence which cannot be related to any luminous impurities. Recent UPS results (Allen, 1983) are in favor of this interpretation (Genet et al., 1984). For the time being, as far as the specific physical properties of pure $ThBr_4$ and $ThCl_4$ are concerned, only the heat capacity measurements versus temperature are progressing, but it would be very interesting to investigate some properties like ferroelectricity and to measure some values like dielectric constant in terms of the temperature. Some delicate NMR experiments at low temperature could be also considered.

4. SPECTROSCOPIC PROPERTIES OF A DOPING ION IN $ThBr_4$ AND $ThCl_4$.

The perfect knowledge of the physical properties of $ThBr_4$ and $ThCl_4$ allowed us to investigate the fundamental relationship : property-structure for a doping ion. The consequence of the special incommensurate phase on the electronic structure of the ion was studied both with lanthanides and actinides elements and through EPR and optical experiments. EPR experiments were achieved using a Brucker Spectrometer operating in X-band or a Varian E-12 spectrometer equipped with an Air Products Helitran cooling system operating in Q-band. Temperature variations were given by a regulated helium gas flow type "Oxfords Instruments cryostat". Optical data were obtained with well shaped and oriented crystals.

Table 9 - Spin hamiltonian parameters for Gd^{3+} in $ThBr_4$ in D_{2d} site (a) and in the charge compensation site (b) Gd^{3+}-n.n.n.v_{Br}- (in units of 10^{-4} cm^{-1}).

$g_{\|\|}$	$g_{\perp}$	g'	b_2^0	b_2^2	b_2^{-2}	b_4^0	b_4^2	b_4^{-2}	b_4^4	b_4^{-4}	b_6^0	b_6^2	b_6^{-2}	b_6^4	b_6^{-4}
a)															
1.992			463			-10			123		-1			3	
b)															
1.994	1.991	-0.001	536.9	85.8	0	-12	-63.8	0	-137	0	-0.6	1.3	0	-7.9	0

$g_z = g_{\|\|}$; $g_x = g_{\perp} + g'$; $g_y = g_{\perp} - g'$.

They were sealed in silica ampoule under about 100 mm of dry helium gas pressure. Absorption spectra were run with a 100 W quartz iodine lamp. Except for selective excitation which was performed with a tunable dye laser, most of the fluorescent studies were done with a mercury vapor lamp or with the laser nitrogen line at 3371 Å. Absorption and emission spectra were recorded from 4 000 cm^{-1} to 33 000 cm^{-1} with a one meter Jobin-Yvon monochromator. The temperature range from 4 K to 300 K was explored with an "Oxford Instruments cryostat". Polarization spectra were classically reported as σ and π, corresponding respectively to an electric vector orientation which was perpendicular and parallel to the four fold optical axis of the crystal. As axial spectra (labelled as α) are similar to the σ ones, we can conclude that only dipolar electric transitions are observed in agreement with what it is expected from 5 f elements.

4.1. E.P.R. Experiments with $ThBr_4$ and $ThCl_4$ doped crystals.

4.1.1. Gd^{3+} in $ThBr_4$:

Gadolinium was chosen as a paramagnetic impurity since the E.P.R. of that ion can even be studied at room temperature. Thus we can follow the behaviour of an E.P.R. line during the phase transition. However, when the trivalent gadolinium ion occupies the tetravalent cation site D_{2d}, it may require a positive charge compensation through Br^- vacancies to maintain the electrical neutrality of the crystal. In the doped crystals, three types of paramagnetic centers were observed : a D_{2d} site and two C_s charge compensation sites (one with vacancies on the nearest Br^- and another on the next nearest Br^-) (Hubert et al., 1982).

To begin with, the spin hamiltonian parameters were calculated at room temperature (Hubert et al., 1984a)from the angular variation of the E.P.R. lines with the magnetic field in the (100) and (001) plane, for the D_{2d} site and one charge compensation site (vacancie on the next nearest neighbour). The corresponding spin hamiltonian parameters are reported in table 9. One can note a large value for b_4^4 which is due to the flat configuration of the nearest Br^- tetrahedron (nn-Br^-) using the superposicion model as a first approximation for the fourth order parameter, we find :

$$b_4^0 = \frac{1}{2}\,\bar{b}_4\,(35\cos^4\alpha - 30\cos^2\alpha + 3)\ ;\quad b_4^4 = \frac{35}{2}\,\bar{b}_4\sin^4\alpha$$

$\bar{b}_4$ is a parameter which characterizes the Gd^{3+} -nnBr^- bonds and α the angle of the bonds with the spin hamiltonian axis. The consequence is a marked anisotropy of the high field line when H is rotated in the (001) plane ($H = H_o + \Delta b_4^4 \cos 4\theta$, with $\theta = (a, H)$. Then, in this plane with $\theta \sim 30°$, the lineshape will be very sensitive to the motion of the Br^- ions during the phase transition

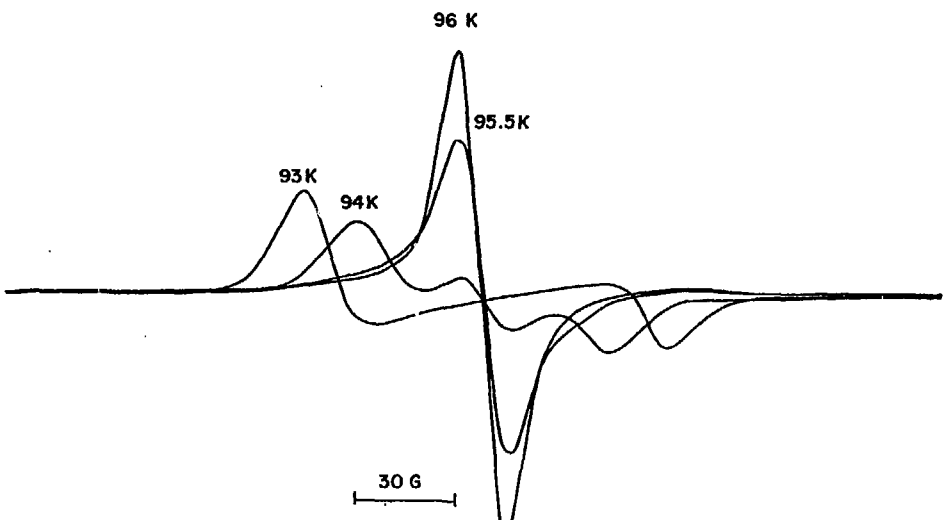

Fig. 18 - Lineshape above and near $T_c \sim 94$ K for $\theta = 22° 30'$. On cooling in the range $T_c + \varepsilon < 96$ K, the line becomes markedly Lorentzian.

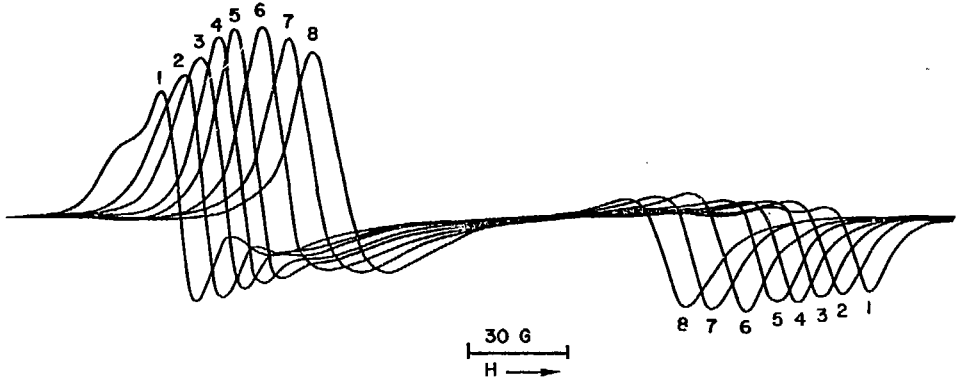

Fig. 19 – Edge singularities for $\Theta = 22° 30$.
$T_1 = 79{,}4$ K ; $T_2 = 84$ K ; $T_3 = 85$ K ; $T_4 = 86$ K ; $T_5 = 87$ K ;
$T_6 = 90$ K ; $T_7 = 91{,}8$ K ; $T_8 = 93$ K.

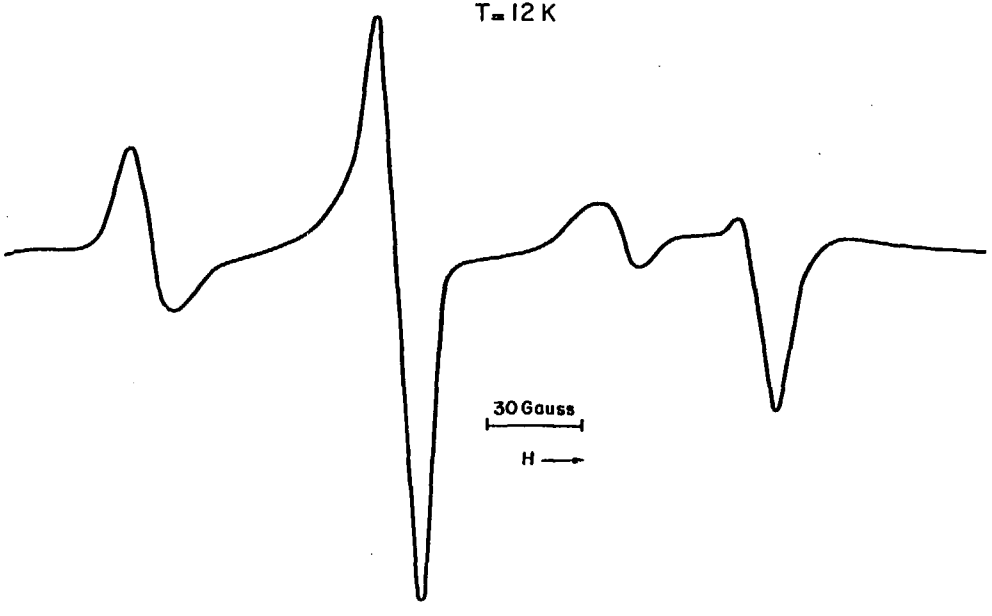

Fig. 20 - Structure of the edge singularity at low temperature T < 80 K. Appearance of a third line like commensurate.

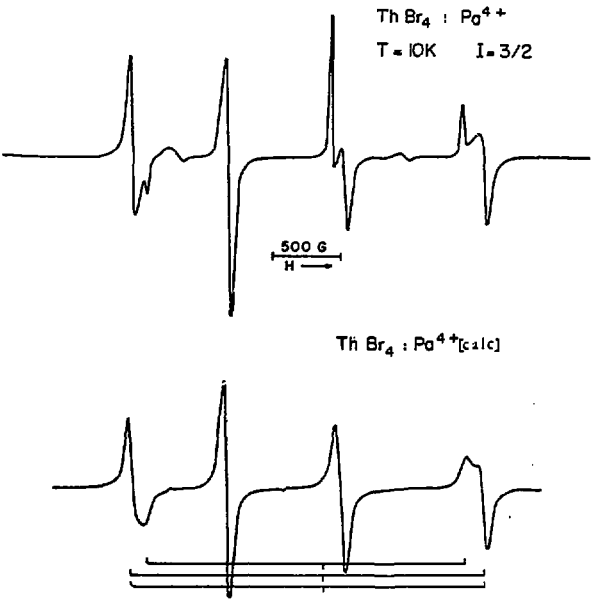

Fig. 21 - Experimental and calculated EPR spectrum of Pa^{4+} : $ThBr_4$.

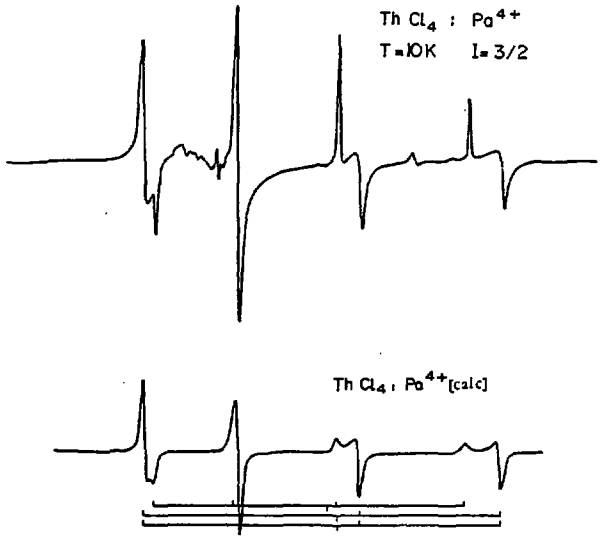

Fig. 22 - Experimental and calculated EPR spectrum of Pa^{4+}: $ThCl_4$.

and will give informations about the motion of the Br^- ions, the critical exponent and the dynamics of the incommensurate phase. The EPR lineshape which is gaussian above the phase transition temperature, becomes broader and markedly lorentzian when cooling in the range $T_c + \varepsilon < 96$ K. Then the line split in two edge singularities from 94 K to 80 K and afterwards a third line appears, starting from the low frequency singularity. The behaviour of the lineshape can be described in three steps.

1 - The pretransitional behaviour (figure 18) gives information about the dynamics of the phase transition. The appearance of the edge singularities when the high temperature line remains on 3 K, could be attributed to a floating phase which is in competition with the static phase.

2 - At lower temperature ($93 < T < 80$ K)(figure 19), the splitting increases with the decreasing of the temperature. From the behaviour of the edge singularities in relation to the temperature, we can deduce the rotation angle of the Br^- ions during the transition $\alpha = 2° 10'$ and the critical exponent $\beta = 0.34 \pm 0.02$. These results are in good agreement with the Raman and neutron scattering measurements.

3 - At very low temperature ($T < 80$ K) (figure 20), a third line rises up from the low field singularity and becomes commensurate. The field modulation ΔH can be expressed with the field displacement $u = \eta \cos \Phi$, with $\eta \sim (T_c - T)^{\beta}$ as $\Delta H = S_1 u + S_2 u^2$. The experimental behaviour of the edge singularities with the appearance of a third line comes up to our expectations when the S_2 term becomes larger than the S_1 term.

The same experiments must be done with $ThCl_4$.

4.1.2. Pa^{4+} in $ThBr_4$ and $ThCl_4$:

Since the E.P.R. of powders of Pa^{4+} in $ThBr_4$ and $ThCl_4$ could be studied only at 4 K, it was not possible to follow the phase transition, but the hyperfine structure study could give one more parameter to the optical data for the calculation of the crystal field parameters.

The parameters of the spin hamiltonian :

$$H = g_{\parallel} \beta H_z S'_z + g_{\perp} \beta (H_x S'_x + H_y S'_y) + A_{\parallel} S'_z I_z + A_{\perp} (S'_x I_x + S'_y I_y)$$

where $S' = \frac{1}{2}$ and $I = \frac{3}{2}$ for ^{231}Pa were obtained by simulation of the spectra shown in figures 21 and 22.

Table 10 - Spin hamiltonian parameters for Pa^{4+} in $ThBr_4$ and $ThCl_4$.

	$\|g_{\parallel}\|$	$\|g_{\perp}\|$	$A_{\parallel}$ (cm^{-1})	$A_{\perp}$ (cm^{-1})
$Pa^{4+}:ThCl_4$	1.605	1.574	0.0556	0.0626
$Pa^{4+}:ThBr_4$	1.616	1.616	0.0571	0.0636

The fact that relatively narrow linewidths are found for these samples suggests that the deviations from D_{2d} symmetry do not greatly affect the magnetic properties of the ground state. Nevertheless, the experimental spectra, especially $ThCl_4 : Pa^{4+}$ show a marked anisotropy of the linewidth. The increase in linewidth could be due to the decrease in symmetry from D_{2d} to D_2 for the modulated structure which could split $g_\perp$ into g_x and g_y. The parameters of the spin hamiltonian are listed in table 10.

4.2. Optical spectroscopy with $ThBr_4$ and $ThCl_4$ doped crystals.

4.2.1. General and theoretical considerations upon the optical data use.

The programme which has been planned for the last ten years was to investigate the electronic structure of the tetravalent actinide ion using $ThBr_4$ and $ThCl_4$ as host matrices. In this outlook, lanthanide ions were studied to give a comparative support, through their isoelectronic structure, to the interpretation upon the 5 f elements.

From this viewpoint, we have always interpreted our data using a classical approach where electronic states resulting from a f^n configuration restricted to D_{2d} symmetry (which is the site symmetry of Th^{4+} ion in $ThBr_4$ and $ThCl_4$) are described with an effective Hamiltonian of the form :

$$H = H_1 + H_2 + H_3$$

where the electrostatic interaction part is given by :

$$H_1 = F_0 + \sum_{k=2,4,6} F^k(5f, 5f) \sum_{i>j=1}^{n} C_i^k C_j^k$$

the spin orbit coupling by :

$$H_2 = \sum_{i=1}^{n} \xi_{5f}\, \ell_i \cdot s_i$$

and the crystal field interaction by :

$$H_3 = B_0^2 C_0^2 + B_0^4 C_0^4 + B_4^4 (C_4^4 + C_{-4}^4) + B_0^6 C_0^6 + B_4^6 (C_4^6 + C_{-4}^6)$$

In the case of the D_2 symmetry provided by the incommensurate structure, the

Table 11 - Absorption wavelengths of Pr^{3+} in $ThBr_4$ at 4.2 K.

$L-S$ state	Wavelength (Å)	Wave number (cm^{-1})	Intensity	polarization
$^3F_2$	19 947	5 011	7	σ
	19 664	5 084	9	σ
	19 453	5 139	10	σ
$^3F_3$	15 553	6 427	4	π
	15 471	6 462	4	σ
	15 377	6 501	4	π
	15 640	6 392	2	σ
$^3F_4$	weak used fluorescence			
$^1G_4$	9 932	10 066	1*bd*	π
$^1D_2$	6 003	16 652	3	σ
	5 987	16 698	5	σ
	5 864	17 047	5	...
	5 859	17 063	5	π
$^3P_0$	4 894	20 428	10	σ
$^3P_1$	4 739	21 098	2	π
	4 718	21 188	9	σ
$^1I_6$	4 760	21 002	1	σ
	4 670	21 405	2	σ
	4 647	21 509	4	σ
$^3P_2$	4 498	22 226	6	σ
	4 470	22 362	6	σ
	4 463	22 398	6	σ

Hamiltonian for the crystal field parameters is :

$$H'_3 = B_2^2 (C_2^2 + C_{-2}^2) + B_2^4 (C_2^4 + C_{-2}^4) + B_2^6 (C_2^6 + C_{-2}^6) + B_6^6 (C_6^6 + C_{-6}^6).$$

A fourth Hamiltonian is sometimes used in a last step for the fitting of the results, it takes into account the configuration interaction parameters : α, β and γ. The calculated energy of the electronic states are obtained through a direct diagonalization of these Hamiltonians.

The matrix elements and the computerized programme are from Berkeley (LBL). They were checked by reproducing several data already published for f^2 configuration.

The r.m.s. (root mean square) associated with the calculated energies is given by :

$$\sigma = \left(\frac{\sum_{i=1}^{N} (E_i(\text{calc.}) - E_i(\text{exp.}))^2}{\text{numbers of levels} - \text{numbers of parameters varied}} \right)^{1/2}$$

The main difficulty encountered in the line assignment for a given spectrum is to detect the pure electronic transition. Most of the time and especially with 5 f elements, intense vibronic transitions are observed, even in a non-centrosymmetric site and the identification of the zero phonon lines is widely improved with help of the polarization effect and with the fluorescence spectra. Both of these experimental facilities are obtained with $ThBr_4$ and $ThCl_4$ whichever ion is studied. Thus, for the latter, we will not discuss in details how each assignment was made for each ion, we will only focus our comment on the final published results. Furthermore, in most cases, the experimental spectra, because of the modulated structure, contain more lines than predicted.

4.2.2. Lanthanide ion studies.

The trivalent lanthanide studies were developped to provide a comparative experimental and theoretical support to the work done on isoelectronic actinide ions. In this view, Pr^{3+} ($4\,f^2$) were firstly examined to help the understanding of the U^{4+} ($5\,f^2$) data.

- Pr^{3+} in $ThBr_4$:

The crystal is doped with about 1 % of Pr by weight. This crystal is pale green and of good optical quality. The absorption lines obtained at 4.2 K are listed in table II. The intense and σ polarized line at 4894 Å was indexed

Table 12 - Laser induced fluorescence of Pr^{3+} in $ThBr_4$ at 77 K. The excitation is into the $^3P_0$ level at 20 473 cm^{-1}.

Wavelength (Å)	Wave number (cm^{-1})	Level (cm^{-1})	Assignment
7461.2	13 399.0	7074	$^3F_4$
7442.9	13 432.0	7041	$^3F_4$
7418.8	13 475.6	6997	$^3F_4$
7399.5	13 510.6	6962	$^3F_4$
7387.0	13 533.6	6939	$^3F_4$
7379.3	13 547.7	6925	$^3F_4$
7364.9	13 574.3	6899	$^3F_4$
6518.0	15 337.0	5136 abs	$^3F_2$
6509.0	15 360.0	5113	$^3F_2$
6496.0	15 390.0	5083 abs	$^3F_2$
6467.0	15 459.0	5014 abs	$^3F_2$
6389.0	15 647.0	4826 .	$^3H_6$
6356.0	15 729.0	4744	$^3H_6$
6309.0	15 845.0	4628	$^3H_6$
6280.0	15 919.0	4554	$^3H_6$
6272.0	15 941.0	4532	$^3H_6$
6263.0	15 963.0	4510	$^3H_6$
6237.0	16 028.0	4445	$^3H_6$
6206.0	16 108.0	4365	$^3H_6$
6195.0	16 138.0	4335	$^3H_6$
6168.0	16 207.0	4266	$^3H_6$

Table 13 - Observed and calculated energy levels of Pr^{3+} in $ThBr_4$.

Levels			
L–S state	Obs. (cm^{-1})	Calc. (cm^{-1})	Irreducible representation
$^3H_4$	0.0	49	5
	188	200	
	300	203	4
	345	266	
	377	358	
	499	391	5
	543	496	
$^3H_5$		2170	
		2210	
		2265	5
		2298	
		2327	5
		2431	
		2471	5
		2539	
$^3H_6$	4266	4259	5
	4335	4337	
	4365	4439	
	4445	4449	5
	4510	4483	
	4532	4549	
	4554	4553	
	4628	4624	
	4744	4706	5
	4826	4732	
$^3F_2$	5113	5143	5
	5011	5149	
	5084	5159	
	5139	5212	
$^3F_3$		6483	5
		6520	
	6501	6557	5
		6565	
		6571	

Levels			
L–S state	Obs. (cm^{-1})	Calc. (cm^{-1})	Irreducible representation
$^3F_4$	6889	6834	
	6925	6904	5
	6935	6945	
	6962	7015	
	6997	7029	
	7041	7081	5
	7074	7112	
$^1G_4$		9581	
		9792	5
		9816	
		9830	
		9921	
	10066	10067	5
		10221	
$^1D_2$	16652	16715	
	16697	16741	
	17063	16933	5
	17047	17099	
$^3P_0$	20425	20447	
$^3P_1$	21098	21037	5
	21158	21120	
$^1I_6$		21136	
		21145	
		21295	5
		21315	
$^1I_6$	21405	21328	
		21517	5
	21509	21560	
		21728	
		21739	5
		21766	
$^3P_2$	22226	22236	
		22291	5
	22362	22323	
	22398	22410	
$^1S_0$		47068	

Table 14 - Parameters obtained from fitting of Pr^{3+} levels in $ThBr_4$ and $ThCl_4$.

Pr^{3+} - $ThBr_4$		Pr^{3+} - $ThCl_4$	
F^2	68354	F^2	68133.2
F^4	50310	F^4	50241.5
F^6	33799	F^6	33584.6
F^0	11558	F^0	11298
ξ	738.8	ξ	746.2
α	21.26 fixed	α	21
$\beta/12$	-66.67 fixed	$\beta/12$	-48
γ	1342.9 fixed	γ	1378
B_0^2	260.0	B_0^2	501.8
B_0^4	-644.2	B_0^4	-603.6
B_4^4	929.2	B_4^4	897.8
B_0^6	1089.0	B_0^6	1396.6
B_4^6	240.6	B_4^6	581.7
42 levels rms = 61 cm^{-1}		49 levels rms = 29 cm^{-1}	

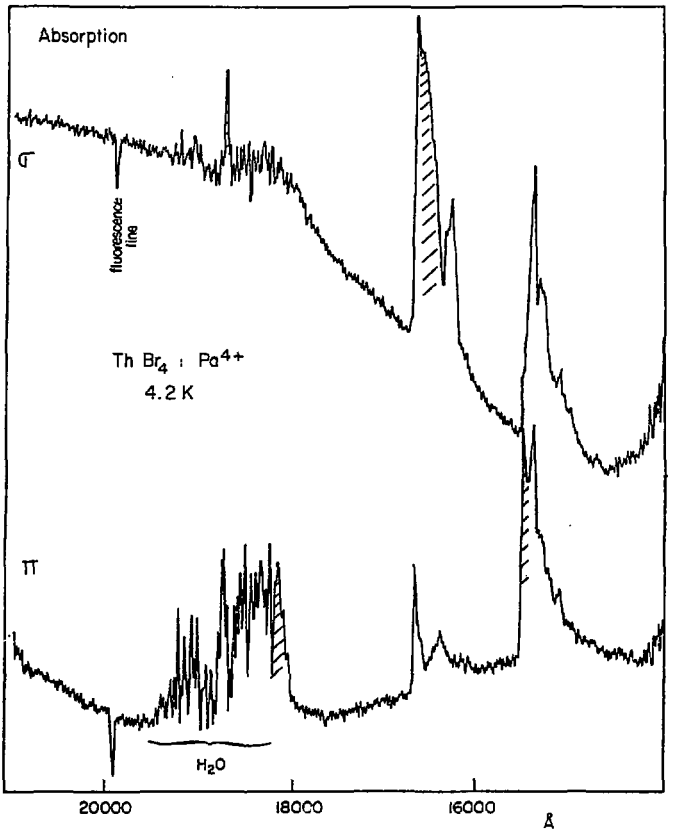

Fig. 23 - Polarized absorption spectra of Pa^{4+} in $ThBr_4$ at 4.2 K.

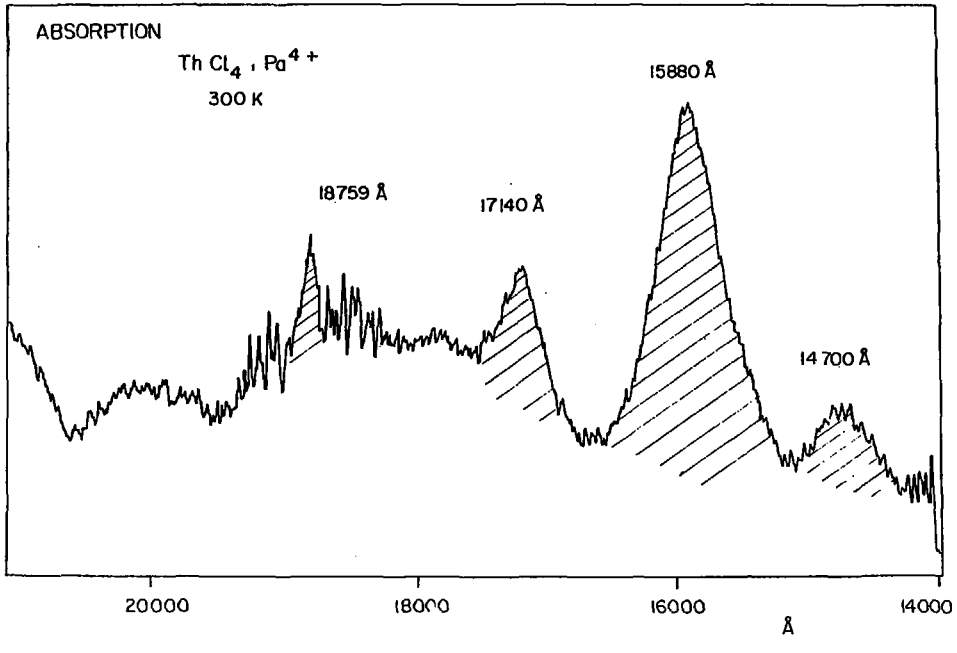

Fig. 24a- Absorption spectra of Pa^{4+} in $ThCl_4$ at 300 K.

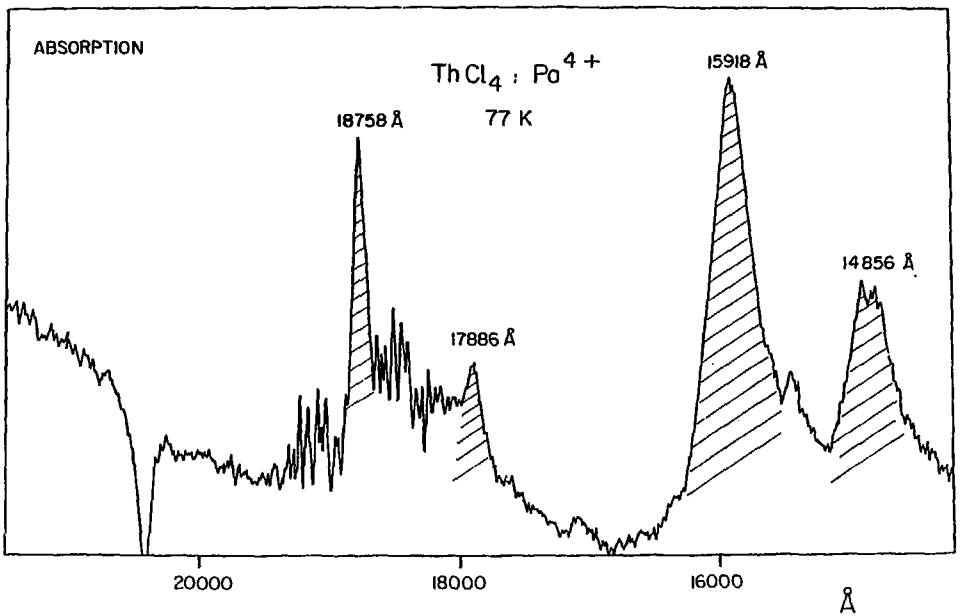

Fig. 24b - Absorption spectra of Pa^{4+} in $ThCl_4$ at 77 K.

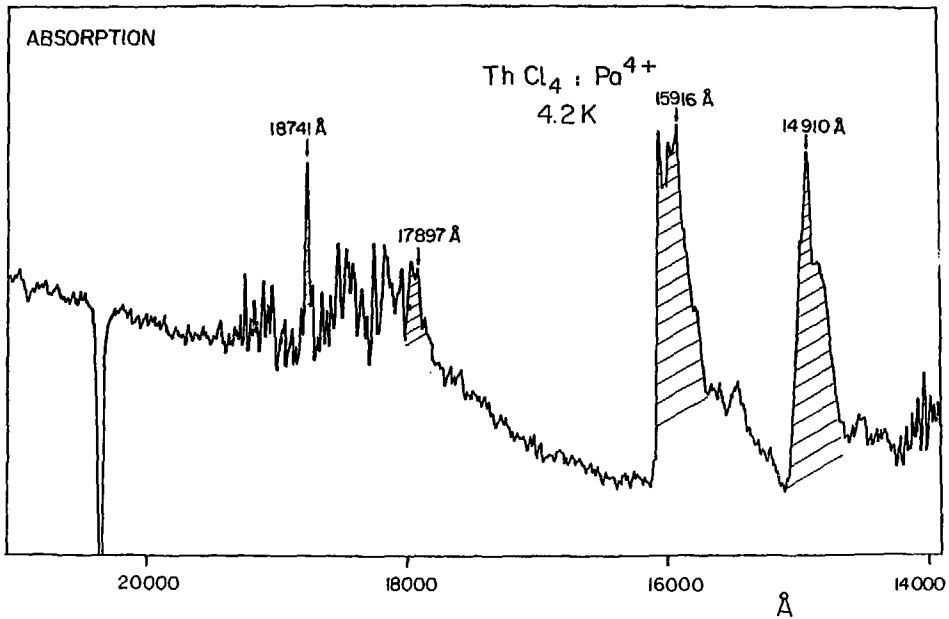

Fig. 24c - Absorption spectra of Pa^{4+} in $ThCl_4$ at 4.2 K.

as the $^3P_0$ level, the ground state being labelled as a Γ_5.

The fluorescence of Pr^{3+} was induced by excitation into the $^3P_0$ level at 20 473 cm^{-1} ; observed lines are reported in table 12. The fit was first made using crystal field parameters given for Pr^{3+} in $LiYF_4$. The calculated energy values for Pr^{3+} in $ThBr_4$ (Conway et al., 1981) are listed in table 13. The associated parameters and their values are given in table 14. This fit is in poor agreement with what is usually obtained for Pr^{3+}, the main cause being the charge compensation which can gives other site symmetries than D_{2d}. These results are now reviewed in terms of perturbation brought by the modulated structure (this point was unknown when the first data were published).

- Pr^{3+} in $ThCl_4$:

A comparison is also under consideration with the study of a Pr^{3+} doped $ThCl_4$ crystal. The first fit obtained, using the same assignment method as for $ThBr_4 : Pr^{3+}$, leads to a set of values given in table 14 (Khan Malek and Krupa, 1983). Selective excitation experiments are planned on both crystals to find out to which site a given absorption or emission line is associated. Several other $ThBr_4$ and $ThCl_4$ crystals have been doped with Nd^{3+}, Eu^{3+}, Yb^{3+}. They haven't been studied yet.

4.2.3. Actinide ion studies.

- Pa^{4+} in $ThBr_4$ and in $ThCl_4$.

The crystals are very well shaped and contain about 0.1 % of protactinium by weight. They are yellow for the bromide host and pale green for the chloride. As expected from a f^1 ion, the absorption spectrum is restricted to few lines, mostly located in the near infrared range. Polarization and temperature effects have been investigated for both crystals. The former are illustrated by the spectrum of $ThBr_4 : Pa^{4+}$ at 4.2 K (Foyentin, 1983), (Krupa et al., 1983a) (figure 23), while the latter are shown in figure 24 on the α-spectrum of $ThCl_4 : Pa^{4+}$ (Krupa et al., 1982). We can see a line (λ = 17 140 Å at 300 K) whose intensity depends on the temperature. The same phemenon was observed with $ThBr_4 : Pa^{4+}$ (λ = 17530 Å at 300 K). This striking similitude between both spectra at 4.2 K is emphasized by the observation of two emission lines at 4 310 and 5 022 cm^{-1} for $ThBr_4 : Pa^{4+}$ and at 4 078 and 4 915 cm^{-1} for $ThCl_4 : Pa^{4+}$. The fluorescence of the 5 022 cm^{-1} and 4 915 cm^{-1} lines is directly produced by the quartz halogen lamp used for the absorption. They are easily seen in figures 23 and 24. This fluorescence of tetravalent protactinium has never been mentioned

Table 15 - List of experimental and calculated energies of Pa^{4+} in $ThBr_4$ and $ThCl_4$.

	$Pa^{4+}:ThCl_4$		$Pa^{4+}:ThBr_4$		
L-S state	Obs. (cm^{-1})	Calc. (cm^{-1})	Obs. (cm^{-1})	Calc. (cm^{-1})	Irreducible representation
$^2F_{5/2}$	0	21.8	0	19.9	Γ_8
	423	408.8	322	313.9	Γ_7
	1260	1252.7	954	940.5	Γ_8
$^2F_{7/2}$	5338	5312.4	5344	5324.3	Γ_8
	5590	5605.8	5517	5522.6	Γ_7
	6286	6291.3	6021	6026.0	Γ_8
	6711	6715.1	6458	6464.8	Γ_7

Table 16 - Spin-orbit and crystal field parameters obtained from fitting of the optical data.

Parameters[a]	$Pa^{4+}:ThCl_4$ (cm^{-1})	$Pa^{4+}:ThBr_4$ (cm^{-1})
ζ	1524.2±5	1532.8±5
B_0^2	−1404.8±50	−1046.5±52
B_0^4	1749.4±94	1366.3±138
B_4^4	−2440.3±98	−1990.1±102
B_0^6	−2404.2±607	−1162.0±541
B_4^6	−194.5±267	623.1±174

Table 17 - Comparison of g values obtained from EPR and optical data.

	EPR		Optical	
	$g_{\|\|}$	$g_{\perp}$	$g_{\|\|}$	$g_{\perp}$
$ThBr_4 : Pa^{4+}$	1,616	1,616	1,296	1,381
$ThCl_4 : Pa^{4+}$	1,605	1,574	1,249	1,203

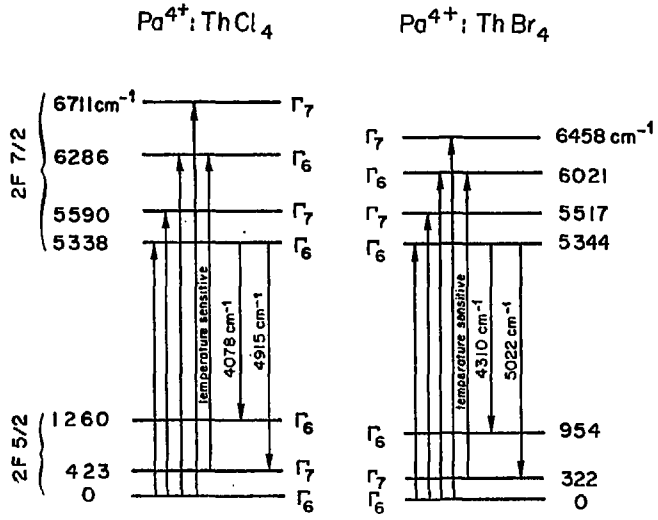

Fig. 25 - Energy level diagrams for Pa^{4+} in $ThBr_4$ and $ThCl_4$.

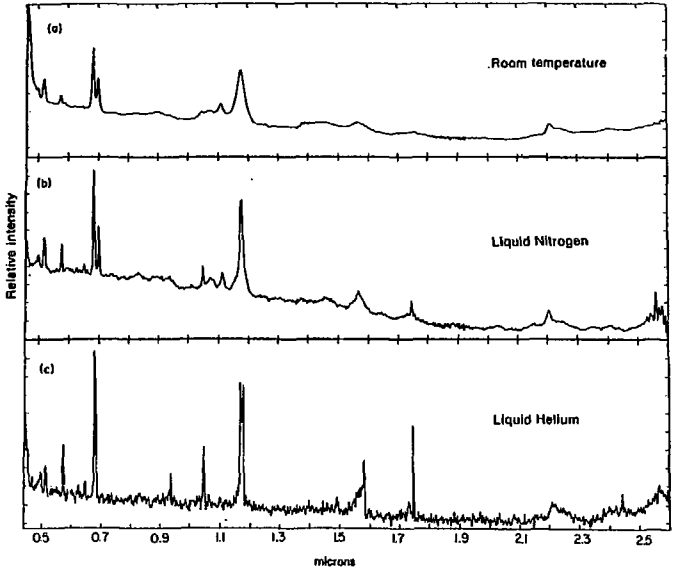

Fig. 26 - Absorption spectra of U^{4+} in $ThBr_4$ at various temperatures.

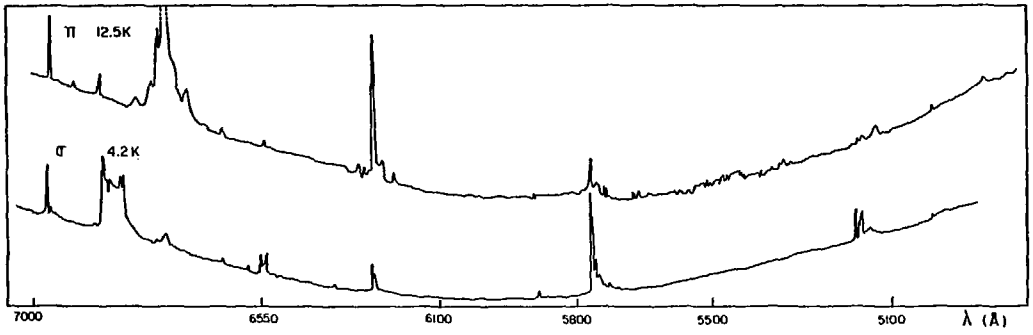

Fig. 27 - Polarized absorption spectra of U^{4+} in $ThBr_4$ in the visible range.

previously, it is temperature dependent and it is quenched at $\sim$ 100 K for $ThBr_4$ and $\sim$ 110 K for $ThCl_4$.

Taking into account all these experimental information, the transitions from the ground crystal field state (J = 5/2) to the four crystal states of the excited J = 7/2 multiplet were assigned. The energy levels of the seven Kramers doublet were calculated in the D_{2d} site symmetry, the values compared to the experimental one are given in table 15 and their associated parameters are reported in table 16. We notice that the spin orbit coupling value is very close to those determined by Amberger (1981) for $PaCl_4$. As one would expect, the crystal field values for $ThCl_4$: Pa^{4+} are larger than for $ThBr_4$: Pa^{4+}. The resulting scheme energy levels for Pa^{4+} in $ThBr_4$ and $ThCl_4$ is shown in figure 25.

From this optical data analysis, the calculations of $g_{||}$ and $g_{\perp}$ for the ground state were made and are in agreement with those given by the EPR measurements (table 17).

Comparison with other optical data concerning Pa^{4+} is quite inefficient since only two papers have been reported. One of them, by Axe (1960), dealing with optical and magnetic data is Cs_2ZrCl_6 : Pa^{4+} with an octahedral site symmetry, the second, recently given by Amberger (1981), deals with a reexamination of the crystal field calculations concerning the $5f^1$ configuration.

- U^{4+} in $ThBr_4$ and in $ThCl_4$.

Among tetravalent actinide ions, U^{4+} was one of the most intensively studied in pure as in doped crystals. If we restrict our purpose to the D_{2d} symmetry, we find two main types of published studies : one of them concerns UCl_4 (Laughlin, 1962), (Hecht and Gruber, 1974 and 1975), (Khan Malek, 1981), the second done with silicate matrices by Richman et al. (1967), Mackey et al. (1975) and Vance and Mackey (1978). The discrepancies between these various works were so important that we took advantage of our study on $ThBr_4$ and $ThCl_4$ to make a further analysis of the uranium (+4) electronic structure. $ThBr_4$: U^{4+} (Genet et al., 1977b) was more widely investigated than $ThCl_4$: U^{4+} (Krupa et al., 1983b), the latter giving us a permanent facility to check the theoretical model developped on $ThBr_4$. Besides these studies with thorium halides, reexamination of U^{4+} in UCl_4 (Khan Malek, 1981) and in $ThSiO_4$ (Khan Malek and Krupa, 1983) is under consideration at Orsay, but the corresponding data will not be reported here. The axial absorption spectra of $ThBr_4$: U^{4+} at various temperature are shown in figure 26. The σ and π polarized spectra for $ThBr_4$: U^{4+} are reported in figure 27.

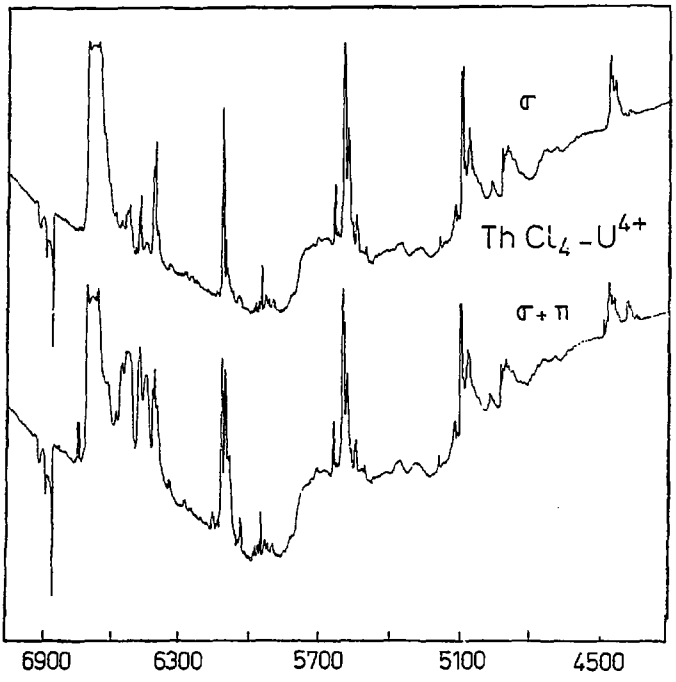

Fig. 28 - Polarized absorption spectra of U^{4+} in $ThCl_4$ at 4.2 K, in the visible range.

Table 18 - Emission spectrum of U^{4+} in $ThBr_4$ at 4.2 K with excitation by the 3 663 Å mercury line.

Exposure times: 15 min			5 h	
Wavelength (Å)	Energy (cm^{-1})	Comments	Wavelength (Å)	Energy (cm^{-1})
5182	19 292	str br	5171	19 333
		br		
5198	19 233	str shp		
5203	19 214	wk		
5213	19 177	str br		
5222	19 144	shp		
5231	19 111	shld		
5239	19 082	str br		
5270	18 970	wk shp		
5289	18 909	wk br		
			5313	18 817
			5366	18 636
			5372	18 610
5444	18 364	str shp		
5454	18 330	str shp		
			5478	18 250
			5487	18 226
			5509	18 147
			5563	17 971
			5754	17 374
			5760	17 356
			5862	17 063
			5883	16 993
			5934	16 847
5913	16 907	med		
			5957	16 782
			6177	16 185
			6236	16 032
			6360	15 719
6440	15 524	wk shp		
			6454	15 496
			6509	15 359
			6519	15 335
6573	15 210	str br		
6582	15 189	shld		
6587	15 177	str br		
		br b		
6611	15 122	str br		
6622	15 097	wk br		
			6729	14 857
			6850	14 594
			6887	14 516
			6914	14 459
			6932	14 422
6941	14 403	shp		
6958	14 368	shp		
6965[c]	14 354	str br		
		br b		
6996	14 290	str shp		
7021	14 239	str br		
7029	14 223	str shp		
7036	14 209	wk shp		
			7051	14 178
7068	14 144	str br		

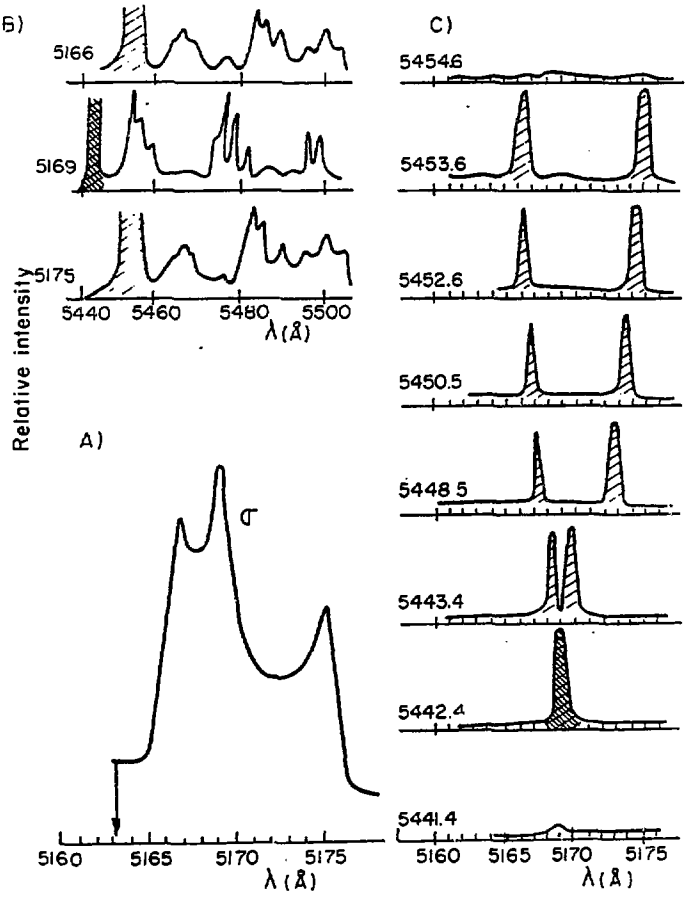

Fig. 29 - A) Typical absorption σ polarized spectrum of U^{4+} in $ThBr_4$.

B) Emission spectra of U^{4+} in $ThBr_4$ by pumping at 5166, 5169 and 5175 Å.

C) Emission spectra of U^{4+} in $ThBr_4$, correlation between excitation and emission lines.

Table 19 - Experimental and calculated energy values (in cm^{-1}) for U^{4+} in D_{2d} sites of $ThBr_4$.

Γ	E calc	E obs	Γ	E calc	E obs	Γ	E calc	E obs
4	0	0	5	8506	8513	1	15229	15204
5	109	78	1	8759	–	5	15389	15412
1	148	–	5	8829	–	2	15587	–
3	657	–	4	8959	–	1	15821	–
2	707	–	2	9086	–	4	15867	–
1	864	–	1	9199	9250	5	16052	16003
5	980	943	3	9450	–	3	16667	–
3	3704	–	5	9483	9530	2	17001	16997
5	3863		4	10587	–	5	17313	17335
4	3942		1	10614	10593	1	19285	19311
1	4025		5	10668	10658	5	19344	19341
3	5624		3	10773	–	3	19433	–
5	5727	5730	5	10961	–	5	19991	19970
2	5790		4	11061	–	4	20023	–
4	6018		3	11137	–	2	20027	–
5	6104		2	11142	–	5	20387	20382
5	6421	6450	1	11451	–	1	20446	20460
1	6556		5	11828	–	3	20827	–
2	6561		3	14313	–	4	20938	–
5	8277	8246	4	14358	–	3	21558	–
3	8307	–	1	14392	14368	5	21813	21842
2	8329	–	5	14632	14654	1	22229	22220
4	8390	–	1	14940	14899	4	22306	–
						1	38522	–

Table 20 - Experimental and calculated energy values (in cm^{-1}) for U^{4+} in D_2 sites of $ThBr_4$.

Γ	E_{calc}	E_{obs}
2	0	0
3	73	10
4	166	146
1	171	-
1	657	-
2	727	-
1	881	-
3	994	967
4	1020	1010
1	3707	-
3	3849	-
4	3860	-
2	3943	-
1	4037	-
1	5608	-
4	5707	5726
3	5728	5734
2	5778	-
2	5995	-
4	6054	-
3	6107	-
4	6384	6328
3	6436	-
1	6558	-
2	6561	-
3	8247	8246
4	8262	8248
1	8288	-
2	8307	-

Table 20 (continued)

Γ	E_{calc}	E_{obs}
2	8386	-
3	8498	8470
4	8507	8552
1	8779	-
3	8827	-
4	8865	-
2	8961	-
2	9106	-
1	9207	9250
1	9459	9499
4	9499	9530
3	9510	9560
2	10570	-
1	10576	10584
3	10647	10652
4	10669	10656
1	10753	-
3	10882	-
4	11001	-
2	11017	-
1	11097	-
2	11121	-
1	11444	-
3	11830	-
4	11864	-
1	14276	-
2	14329	-
1	14409	14364
4	14601	14612
3	14646	14709
1	14969	14915

Table 20 (continued)

Γ	E_{calc}	E_{obs}
1	15211	15207
3	15394	15392
4	15396	15421
2	15591	-
1	15817	-
2	15926	-
4	16047	16003
3	16058	16013
1	16720	-
2	17017	17006
4	17320	17347
3	17356	17368
1	19293	19302
3	19330	19318
4	19382	19352
1	19454	-
4	19913	19942
2	19971	-
3	20086	-
2	20091	-
3	20349	-
4	20449	-
1	20454	20460
1	20871	-
2	20980	-
1	21568	-
4	21728	-
3	21847	21838
1	22225	22220
2	22318	-
1	38680	-

Table 21 - Associated parameters for U^{4+} in $ThBr_4$ (D_{2d} and D_2 sites) from fitting of the optical data.

	U^{4+} : $ThBr_4$	
	D_{2d}	D_2
F^2	42253 ± 127	42264 ± 84
F^4	40458 ± 489	41159 ±407
F^6	25881 ± 383	26018 ±237
ζ	1783 ± 7	1774 ± 5
α	31 ± 1	[31]
β	-644 ± 75	[-644]
γ	[1200]	[1200]
α'	-	-
β'	-	-
γ'	-	-
M^0	[0.99]	[0.99]
M^2	[0.55]	[0.55]
M^4	[0.38]	[0.38]
P^2	[500]	[500]
P^4	[500]	[500]
P^6	[500]	[500]
B_0^2	-1096 ± 80	-1108 ± 65
B_0^4	1316 ± 146	1358 ±137
B_4^4	-2230 ± 85	-2219 ± 76
B_0^6	-3170 ± 379	-3458 ±267
B_4^6	686 ± 246	694 ±195
B_2^2	-	-78 ± 30
B_2^4	-	318 ±122
B_2^6	-	136 ±101
B_6^6	-	123 ±125
Number of Levels	26	38
n	36	39

Figure 28 represents the similar spectra for $ThCl_4 : U^{4+}$ for the visible range.

The fluorescence spectrum of U^{4+} was observed for the first time in these matrices. This emission is strongly dependent on temperature and on excitation energy. For $ThBr_4$ crystals excitation at room temperature by a mercury lamp (λ = 3 663 Å) is inefficient but can be obtained with a nitrogen laser (λ = 3371 Å). By cooling down the crystal, fluorescence is observed even with the λ = 3 663 Å mercury line. Results at 4.2 K are given in table 18. Strong and weak lines are reported in relation to exposure time (in this case the fluorescence spectrum was recorded on photograph plates for two different exposure times). it is noticeable that an excitation at λ = 2 534 Å does not induce any fluorescence of U^{4+} though the matrix $ThBr_4$ is highly absorbing in this range. Similar emission was obtained with $ThCl_4 : U^{4+}$.

Detailed studies of the fluorescence through selective excitation experiments have shown that the energy of the emission line could vary continuously. With the exciting wavelength (Delamoye et al., 1983a). This is clearly represented in figure 29 where excitation with a dye laser in the σ band (from 5 165 Å to 5 182 Å) induced a continuous emission from 5 441 Å to 5 453 Å. The main feature being that emission at 5 453 Å produced simultaneously by an absorption at 5 165 Å and 5175 Å results from ions which are in the same site symmetry, while absorption at 5 169 Å leading to a different emission at 5 441 Å is related to a symmetry which is different from the previous one. The experiment accounts for two site symmetries for U^{4+}. This was checked on several other groups of emission lines and also on $ThCl_4 : U^{4+}$ crystals.

This experimental result is directly connected with the incommensurate phase of $ThBr_4$ and $ThCl_4$ at low temperature, where two sites of D_{2d} and D_2 symmetry are involved (see 3.7.). A careful study of the fluorescence spectrum of U^{4+} allowed us to label as D_{2d} or D_2 most of the absorption lines and this leads us to a reexamination of the assignment of the crystal field states of U^{4+} in $ThBr_4$ (Delamoye et al., 1983b) .The calculated and observed energy values for D_{2d} and D_2 are respectively given in tables 19 and 20. The best fit is obtained with parameter values reported in table 21. We notice that four crystal field parameters (B_2^2, B_2^4, B_2^6, B_6^6) have been added to those of D_{2d} for the fitting in D_2 symmetry. It is of interest to note how this way of interpreting these results do not account for the multisite of D_2 symmetry where B_q^k of varying values should be necessary to describe and interpret accurately the energy continuum which exists between the D_2 and D_{2d} absorption lines. The same analysis of the absorption spectra of $ThCl_4 : U^{4+}$ with decomposition into D_2 and D_{2d} sites is under way.

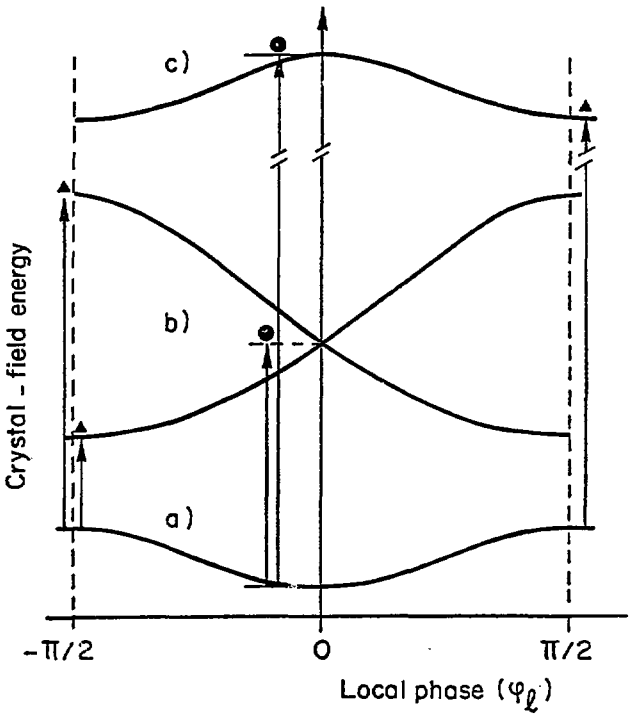

Fig. 30 - Schematic energy levels variations for a singulet-state with $\beta > 0$ (a), a doublet-state with $\beta > 0$ (b) and a singlet-state with $\beta < 0$ (c). Vertical arrows represent the transition corresponding to the edge-singularities (full triangle and circles in connection with fig. 31).

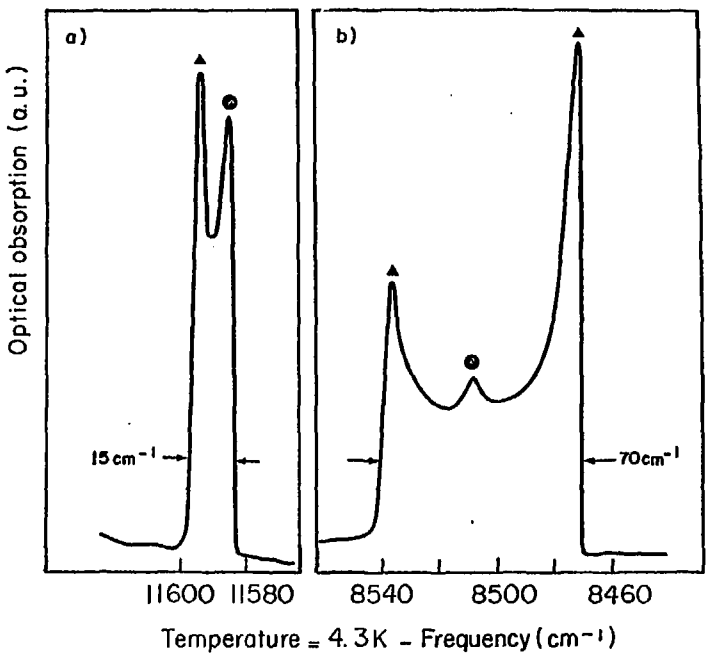

Fig. 31 - Typical absorption spectrum of U^{4+} in $ThBr_4$ at 4.2 K .
(a) π polarization ; (b) σ polarization.

The incommensurate phase of $ThBr_4$ at low temperature is responsible for the appearance of two site symmetries as it was shown previously. The model of the modulated structure which is very well adapted to the determination of energy states can also be used to explain the very special lineshape observed.

It was shown by Delamoye and Currat (1982b) that the energy level j of a U^{4+} ion in a site labelled ℓ in the modulated structure is given by :

$$E^j = E_o^j + \eta^2 \{\alpha_j + \beta_j \sin^2 \varphi_\ell\} \pm \gamma_j \eta \sin\varphi_\ell$$

where α_j, β_j are numerical coefficients, γ_j being zero for the non degenerate states in D_{2d} (Γ_1 to Γ_4), η and φ_ℓ were already described (see 3.7.). Each optical transition between two levels j and j' is related to a frequency ν through :

$$\nu = E_\nu^j - E_\nu^{j'}$$

and the intensity of the transition is connected with ν and φ_ℓ by :

$$I_\nu^{jj'} = \left| \frac{d\nu^{jj'}}{d\varphi_\ell} \right|^{-1}$$

Finally, it is found that the edge singularities correspond to :

$$\frac{dE_\ell^{j'}}{d\varphi_\ell} = \frac{dE_\ell^j}{d\varphi_\ell}$$

The resulting variations of the energy levels with φ_ℓ is reported in figure 30. The corresponding lineshapes are also shown and this theoretical profile is quite similar to those observed for the experimental lines. Some of them are represented in figure 31. The σ-transitions are broader than the π ones as predicted by the model (Delamoye and Currat, 1982b). The lineshapes of $ThCl_4 : U^{4+}$ transitions are of the same profile and though the neutron diffraction of $ThCl_4$ has not been done yet, it is very likely that its structure is incommensurate.

- $\underline{Np^{4+} \text{ in } ThBr_4 \text{ and } ThCl_4}$.

The crystal growth was achieved and the optical spectra were recorded. It seems that we got two oxidation states for the neptunium, namely the trivalent and tetravalent states. Under these conditions, both spectra are not yet assigned.

Table 22 - Experimental and calculated oscillator strengths of U^{4+} transitions in $ThBr_4$.

Level assignment	Energy region (cm^{-1})	Center of band energy (cm^{-1})	$f \times 10^4$ exp.	$f \times 10^4$ cal.
		Cryst.	Cryst.	Cryst.
$^3F_3$, $^3F_4$	7810-10100	8547	2.80	2.84
$^3H_6$	10100-13330	1111	1.05	0.83
$^3P_0$, $^1D_2$, $^1G_4$	13330-16500	14724	2.93	2.87
$^3P_1$	16500-18700	17391	0.99	1.47
$^1I_6$	18700-22200	19342	2.84	2.64
$^3P_2$	22200-25000			0.06
$^1S_0$				0.095
	rms deviation $\times 10^4$			0.40

T_λ ($\times 10^{18}$ s^{-1}) ; $T_2 = 5.6$; $T_4 = 2.2$; $T_6 \simeq 0$.

- Pu^{4+} (?) in $ThBr_4$:

$ThBr_4$ doped crystal with PuO_2 has a bright blue colour, certainly due to Pu^{3+}. It means that the reducing properties of the matrix already observed for neptunium is, for plutonium, much more marked. The spectroscopy of the plutonium doped crystal had never been done previously in the tetravalent state.

4.3. The "up-conversion" phenomenon.

Recently, it was discovered (Genet et al., 1981) that infrared excitation of $ThBr_4$ and $ThCl_4$ crystals doped with U^{4+} or Np^{4+} gives a strong emission in the visible range. This very uncommon anti-Stokes fluorescence is called "up-conversion" and was previously found with 4 f elements (Auzel, 1966a,b), (Auzel, 1973). $ThBr_4$ and $ThCl_4$ enabled us to observe this effect for the first time with actinide ions. We mainly studied $ThBr_4 : U^{4+}$ crystals. We found that the excitation of a single tetravalent uranium ion at room temperature is obtained by absorption of two consecutive infrared photons of 9 540 Å and induces a bright red fluorescence according to a broad band from 6 700 to 7 200 Å. By cooling down the crystal below the phase transition temperature ($T < 95$ K) an additional, but weak, fluorescence in green range ($\lambda \sim 5\ 200$ Å) is observed. The connexion between this green fluorescence with the modulated structure is not yet established, but is very likely. It is noticeable that the fluorescence induced on U^{4+} with two infrared photons or a unique UV photon is the same (see 4.2.3.). The lifetime measurements of the level of the excited U^{4+} ion are under consideration to get a better understanding of the role played by uranium when it acts as an "up-converter" (Hubert et al., 1984 b). From the same point of view, oscillator strengths of U^{4+} in $ThBr_4$ were obtained by graphical integration of absorption spectra at room temperature between 4 500 to 13 000 Å (Auzel et al., 1982). Using the Judd's theory, the determination of the T_λ parameters was done at the same time as the associated oscillator strengths. The latter are compared to the experimental one in table 22. One can note that they are of about 10^{-4} which are two orders of magnitude larger than for the iso-electronic ions Pr^{3+} in the 4 f series ($f \sim 10^{-6}$) (Peacok, 1975). The high value of the U^{4+} oscillator strength is very favourable to the observation of the up-conversion effect while the lifetime of the absorption level should be rather short as predicted by the theory.

5. CONCLUSION.

From the solid state physics to the optical spectroscopy of 5 f elements, we have described in details how $ThBr_4$ and $ThCl_4$ are acting an important role in the applied and basic research field. The possible applications are based on the

scintillation properties of these crystals while the fundamental aspect is related to their special incommensurate structure which modulates the host properties of these matrices at low temperature. This very small perturbation of bromine atom positions have optical consequences on the absorption and emission of the actinide studied ions (Pa^{4+}, U^{4+}, Np^{4+}) which are interpreted in function of the modulated structure parameters determined by inelastic and elastic neutron scattering and by Raman spectroscopy. The structural model proposed shows, for the first time, how the optical properties of the investigated ion are influenced by the sinusoïdal displacements of the bromine atoms, leading to an energy continuum in the absorption and reducing the site symmetry from D_{2d} to a multisite of D_2 symmetry./Though this work, which lasted several years was only focused on two crystals, apparently very common, we don't claim that everything has been done, and we especially think that heat capacity, photoconductivity, ferroelectricity and dielectric constant measurements should be very interesting to investigate. As a philosophical conclusion concerning the scientist facing the science research field, we would like to say that it is as fruitful to accumulate a lot of experimental data on twin pairs of crystals similar to the $ThBr_4$ and $ThCl_4$ set as to use the same experimental device to determine a unique information upon a lot of different compounds.

The scientific story of $ThBr_4$ is not over, it has recently been found by NQR (Guibé et al., 1983) that the α-phase of $ThBr_4$ really exists and can be produced on crystal of large volume. We already know that a lot of properties previously investigated on the β-phase should be reexamined in the view of the new structure which might be still commensurate at helium liquid temperature.

Acknowledgments.

I would sincerely like to thank all the scientists who have participated in this collective research on $ThBr_4$ and $ThCl_4$ for ten years at Orsay in the frame of the work of the 5 f element spectroscopy group, especially : R. Carlier, P. Delamoye, S. Hubert, M. Hussonnois, Ch. Khan Malek, J.C. Krupa, and, for her technical assistance : L. Brillard.

I would also wish to thank Professor R. Guillaumont for his permanent and helpful encouragement in supporting and developping this research area.

At last, I would like to mention that an important part of this work would have not been possible without the collaboration of several French Laboratories ans specially with : F. Auzel, from the CNET (Bagneux), L. Bernard and R. Currat for the ILL (Grenoble), R. de Kouchkovsky for the CEA (Saclay), J. Emery and J.C. Fayet from the University of Le Mans, L. Guibé from the IEF (Orsay),

S. Lefrant from the University of Orsay. Some foreign laboratories also intensively participated in this work and influenced it to a great extent. I would specially thank J. Conway and N. Edelstein from the LBL (Berkeley, California) and K. Rajnak from Kalamazoo (Michigan). Finally, I thank M. Liêbe for her excellent preparation and typing of the manuscript.

Bibliography

Allen, G.C., 1983, Private communication.

Amberger, H.D., W. Grape, E. Stumpp, 1981, Actinides 1981.

Auzel, F., 1966 a, C.R. Acad. Sc. Paris, 262, série B, 1016.

Auzel, F., 1966 b, C.R. Acad. Sc. Paris, 263, série B, 819.

Auzel, F., 1973, Proc. IEEE, 61, 758.

Auzel, F., S. Hubert, P. Delamoye, 1982, J. of Luminescence, 26, 251.

Axe, J.D., 1960, Ph.D. Thesis, UCRL 9293.

Bernard, L., R. Currat, P. Delamoye, C.M.E. Zeyen, S. Hubert, R. de Kouchkovsky, 1983, J. Phys. C : Solid State Phys. 16, 433.

Berzelius, J.J., 1829, Pogg.Ann., 16, 385.

Brown, D., 1968, Halides of Lanthanides and Actinides (J. Wiley) p. 190.

Brown, D., T.L. Hall, P.T. Moseley, 1973, J. Chem. Soc. Dalton Trans. 6, 686.

Blinc, R., I.P. Aleksandrova, A.S. Chaves, F. Milia, V. Rutar, J. Selinger, B. Topic, S. Zummer, 1982, J. Phys. C : Solid State Phys. 15, 547.

Carlier, R., M. Genet, 1972, Radiochimica Acta 18, 16.

Carlier, R., M. Genet, 1975, C. R. Acad. Sc. Paris, 281, C, 671.

Carlier, R., J.C. Krupa, M. Hussonnois, M. Genet, R. Guillaumont, 1977, Nucl. Inst. Meth. 143, 613.

Carter, J.C., 1975, Ph. D. Thesis Warwick Univ. (G.B.).

Conway, J.G., J.C. Krupa, P. Delamoye, M. Genet, 1981, J. Chem. Phys. 74, 849.

Currat, R., 1981, J. de Phys., Colloque C6, 12, 42, 693.

De Kouchkovsky, R., M.F. Le Cloarec, P. Delamoye, 1981, Mat. Res. Bull. 16, 1421.

Delamoye, P., S. Hubert, S. Lefrant, 1982a, in Proc. International Conference on Raman Spectroscopy, Bordeaux, France, 1982, Eds. J. Lascombe and P.V. Huong, John Wiley, New York.

Delamoye, P., R. Currat, 1982b, J. Phys. Lettres, 43, L 655.

Delamoye, P., J.C. Krupa, J.G. Conway, N. Edelstein, 1983a, Phys. Rev. B, 28, 9, 4913.

Delamoye, P., K. Rajnak, M. Genet, N. Edelstein, 1983b, Phys. Rev. B, 28, 9, 4923.

D'Eye, R.W.M., 1950, J. Chem. Soc. 2764.

Elson, R.E., S. Fried, P. Sellers, W.H. Zachariasen, 1950, J. Am. Chem. Soc. 72, 5791.

Foyentin, M., 1983, Thèse 3ème cycle, Orsay, France.

Freund, A., J. Schneider, 1972, J. Crystal Growth, 13, 247.

Genet, M., G. Goby, M. Hussonnois, J.C. Krupa, R. Guillaumont, 1975, Radiochem. Radioanal. Letters, 23, 19.

Genet, M., M. Hussonnois, J.C. Krupa, R. Guillaumont, R. Carlier, 1976a, J. Luminescence, 12/13, 953.

Genet, M., G. Goby, M. Hussonnois, J.C. Krupa, R. Guillaumont, 1976b, Inorg. Nucl. Chem. Letters, 12, 179.

Genet, M., M. Hussonnois, J.C. Krupa, R. Guillaumont, 1977a, Radiochem. Radioanal. Letters, 28, 251.

Genet, M., P. Delamoye, N. Edelstein, J. Conway, 1977b, J. Chem. Phys. 67, 4, 1620.

Genet, M., S. Hubert, F. Auzel, 1981, C.R. Acad. Sc. Paris, 293, Série II, 267.

Genet et al., 1984 (to be published).

Gourdji, M., A. Peneau, M. Genet, L. Guibé, 1983, 7th Intern. Symposium on NQR Spectroscopy, 11-14 juillet 1983, Kingston, Ontario, USA.

Hecht, H.G., J.B. Gruber, 1974, J. Chem. Phys. 60, 4872.

Hecht, H.G., J.B. Gruber, 1975, J. Chem. Phys. 63, 2773.

Hubert, S., P. Delamoye, S. Lefrant, M. Lepostollec, M. Hussonnois, 1981, J. Solid State Phys. 36, 36.

Hubert, S., J. Emery, J.J. Rousseau, J.C. Fayet, 1982, J. Phys. Lettres 43, L 815.

Hubert, S., et al., 1984a, to be published.

Hubert, S., et al., 1984b, to be published.

Hussonnois, M., J.C. Krupa, M. Genet, R. Guillaumont, 1977, Mat. Res. Bull. 12, 643.

Hussonnois, M., J.C. Krupa, M. Genet, L. Brillard, R. Carlier, 1981, J. Cryst. Growth 51, 11

Khan Malek, C., 1981, Thèse 3ème cycle, Orsay, France.

Khan Malek, C., A. Peneau, L. Guibé, P. Delamoye, M. Hussonnois, 1982, J. of Molecular Struct. 83, 201.

Khan Malek, C., J.C. Krupa, 1983, Private communication.

Krupa, J.C., M. Hussonnois, M. Genet, 1976, Inorg. Nucl. Chem. Letters, 12, 571.

Krupa, J.C., M. Genet, M. Hussonnois, R. Guillaumont, 1978, Nucl. Inst. Meth. 151, 405.

Krupa, J.C., M. Hussonnois, M. Genet, R. Guillaumont, 1982, J. Chem. Phys. 77, 154.

Krupa, J.C., S. Hubert, M. Foyentin, E. Gamp, N. Edelstein, 1983a, J. Chem. Phys. 78, 2175.

Krupa, J.C., C. Khan Malek, 1983b, 13èmes Journées des Actinides, Avril 1983, Elat, Israël.

Kovalev, O.V., Irreducible Representations of Space Groups, 1964 (Gordon and Breach, New York).

Kravenchko, E.A., O.M. Ionova, E.G. Il'in, 1975, Russ. J. Inorg. Chem. 20, 1416.

Laughlin, Mac R., 1962, J. Chem. Phys. 36, 2699.

Mackey, D.J., W.A. Runciman, E.R. Vance, 1975, Phys. Rev. B, 11, 211.

Mason, J.T., M.C. Jha, P. Chiotti, 1973, J. Less Com. Met. 34, 143.

Mason, J.T., M.C. Jha, D.M. Bailey, P. Chiotti, 1974, J. Less Com. Met. 35, 331.

Mentz, F.H., 1979, Thèse 3ème cycle Orsay, France.

Mooney, R.C.L., 1949, Acta Cryst. 2, 189.

Mucker, K., G.S. Smith, Q. Johnson, R.E. Elson, 1969, Acta Cryst. B 25, 2362.

Nilson, L.F., 1882, Ber. 95, 2437.

Peacock, R.D., 1975, Structure and Bonding (Springer Verlag, Berlin, Heidelberg, New York) 22, 83.

Pynn, R., 1979, Nature 281, 433.
Rand, J., 1975, Atomic Energy Review (special issue), 5, 28.
Reddock, A.H., 1961, J. Chem. Phys. 35, 1085.
Richman, J., P. Kisliuk, E.Y. Wong, 1967, Phys. Rev. 155, 262.
Scalfe, D.E., 1966, Inorg. Chem. 5, 162.
Troost and Ouvrard, 1889, Ann. de Chimie et de Physique, XVII, 227.
Vance, E.R., D.J. Mackey, 1978, Phys. Rev. B 18, 185.